JOURNAL OF PETROLOGY | VOLUME 47 | NUMBER 4 | PAGES 745–771 | 2006 | doi:10.1093/petrology/egi092

# Discontinuous Melt Extraction and Weak Refertilization of Mantle Peridotites at the Vema Lithospheric Section (Mid-Atlantic Ridge)

**DANIELE BRUNELLI[1,2,*], MONIQUE SEYLER[3], ANNA CIPRIANI[4], LUISA OTTOLINI[5] AND ENRICO BONATTI[1,4,6]**

[1]ISTITUTO DI SCIENZE MARINE, GEOLOGIA MARINA, CNR, VIA GOBETTI 101, 40129 BOLOGNA, ITALY

[2]LABORATORIE P. SÜE, CEA-CNRS, BÂT. 637, GIF SUR YVETTE, 91191, FRANCE

[3]LABORATOIRE DE MINÉRALOGIE–PÉTROLOGIE, UMR 7160 CNRS–MUSÉUM NATIONAL D'HISTOIRE NATURELLE, 61 RUE BUFFON, PARIS 75005, FRANCE

[4]DEPARTMENT OF EARTH AND ENVIRONMENTAL SCIENCES, LAMONT DOHERTY EARTH OBSERVATORY, COLUMBIA UNIVERSITY, PALISADES, NY 10964, USA

[5]ISTITUTO DI GEOSCIENZE E GEORISORSE, SEDE DI PAVIA, CNR, VIA FERRATA 1, 27100, PAVIA, ITALY

[6]DIPARTIMENTO DI SCIENZE DELLA TERRA, UNIVERSITÀ 'LA SAPIENZA', PIAZZALE ALDO MORO 5, 00187, ROME, ITALY

**RECEIVED OCTOBER 27, 2004; ACCEPTED NOVEMBER 16, 2005; ADVANCE ACCESS PUBLICATION DECEMBER 22, 2005**

*Melting processes beneath the Mid-Atlantic Ridge were studied in residual mantle peridotites sampled from a lithospheric section exposed near the Vema Fracture Zone at 11°N along the Mid-Atlantic Ridge. Fractional and dynamic melting models were tested based on clinopyroxene rare earth element and high field strength element data. Pure fractional melting (non-modal) cannot account for the observed trends, whereas dynamic melting with critical mass porosity <0·01 fits better the measured values. Observed microtextures suggest weak refertilization with 0·1–1% quasi-instantaneous or partially aggregated melts trapped during percolation. The composition of the melts is evaluated, together with their provenance, with respect to the garnet–spinel transition. Partial melts appear to be aggregated over short but variable intervals of the melting column. Deep melts (generated within the garnet stability field at the base of the melting column) escape detection, being separated from the residues by transport inside conduits or fractures. The temporal evolution of the melting process along the exposed section shows a steady increase of mantle temperature from 20 Ma to present.*

KEY WORDS: *mantle partial melting; abyssal peridotite; trace element; refertilization; Vema Fracture Zone*

## INTRODUCTION

The generation of oceanic crust through partial melting of upwelling mantle peridotite beneath mid-ocean ridges is an important process in the evolution of our planet. Although many studies have focused on this process, some aspects are poorly understood. This paper addresses two such aspects. One is an attempt to define the melting process in terms of fractional and dynamic melting versus mantle porosity, and of melt–solid reactions within the mantle during percolation. The other aims at clarifying temporal variations in the melting process at a single segment of a slow-spreading ridge. Both these problems are approached through the study of the elemental geochemistry of abyssal peridotites.

This study is based on a set of samples of mantle peridotite obtained at closely spaced intervals along a 300 km long section of oceanic lithosphere exposed on the sea floor south of the Vema Transform, on the Mid-Atlantic Ridge at 11°N. This section represents a 20 Myr interval of formation of oceanic lithosphere at a single ridge segment.

*Corresponding author. Present address: Laboratoire P. Süe, CEA–CNRS, Gif sur Yvette, 91191 France. Telephone: +33 16908 9522. Fax: +33 16908 6923. E-mail: daniele.brunelli@bo.ismar.cnr.it

© The Author 2005. Published by Oxford University Press. All rights reserved. For Permissions, please e-mail: journals.permissions@oxfordjournals.org

Downloaded from http://petrology.oxfordjournals.org/ at Kainan University on March 17, 2015

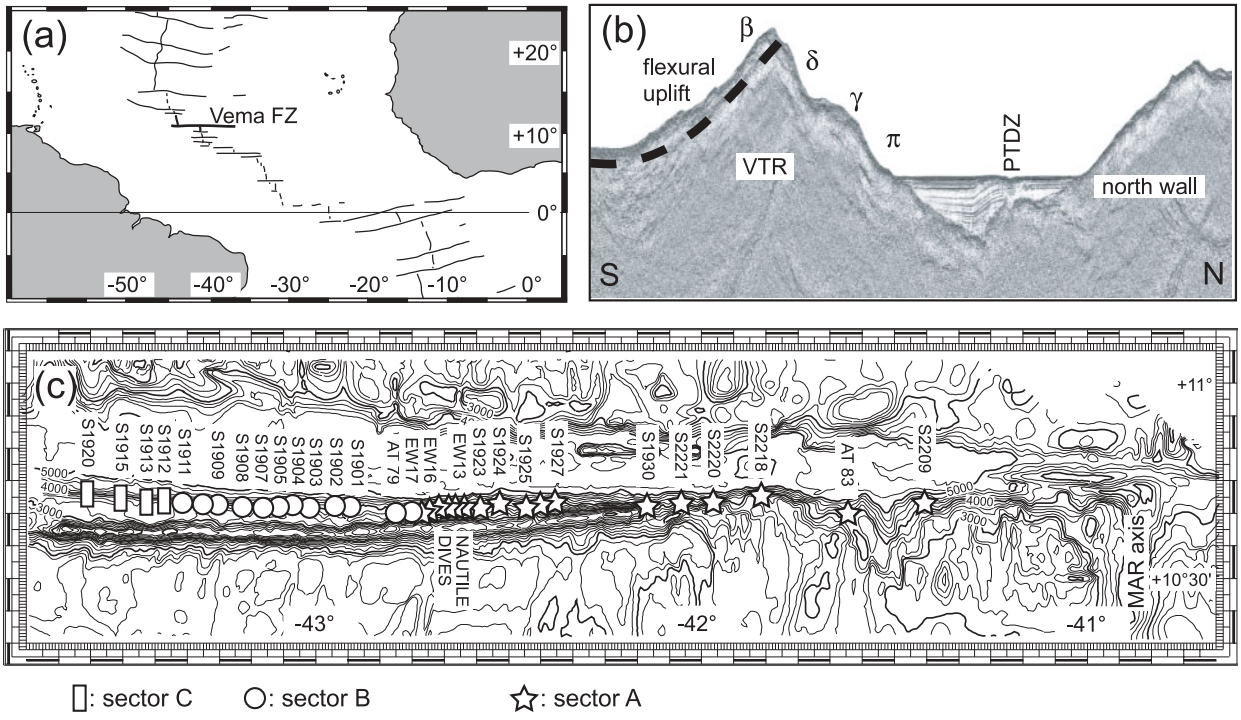


**Fig. 1.** Location and morphology of the Vema Fracture Zone region. (a) Location of the Vema Fracture Zone on the Mid-Atlantic Ridge. (b) Structural interpretation of the Vema Lithospheric Section exposure superimposed on a north–south seismic profile at 42°42′W in correspondence to the *Nautile* dive sites (Auzende *et al.*, 1989). The lithospheric flexure of the southern wall is shown by the deformation of the reflector marking the base of the basaltic layer (dashed line). Also reported are the lithological units according to Auzende *et al.* (1989): π, peridotites; γ, gabbros; δ, dolerites of the dike complex; β, basalts and basaltic breccias; PTDZ, Principal Transform Displacement Zone, interpreted as trace of the transform fault. (c) Bathymetric map of the Vema Fracture Zone. The southern wall exposes a 300 km long continuous section of oceanic crust (Vema Lithospheric Section). Sampling sites are grouped in three distinct sectors according to petrography (see text).

## GEOLOGICAL SETTING

The Vema Fracture Zone (VFZ) is one of the large offset transform faults inherited from the opening of the Central Atlantic (Fig. 1a). It offsets the Mid-Atlantic Ridge (MAR) at 11°N by 310 km in a sinistral sense, giving an age contrast of ~20 Ma. The MAR from the Equator to about 20°N appears to have 'normal' topography and zero-age basalt composition, except for anomalous regions at 2–3°N (Bonatti *et al.*, 1993) and 14–17°N that were perhaps affected by mantle plumes (Dosso *et al.*, 1991, 1993). We have no evidence of plume interaction with the MAR in the vicinity of the Vema transform.

The southern side of the Vema transform valley is characterized by the presence of a prominent Transverse Ridge (Vema Transverse Ridge or VTR) running parallel to the transform valley. The VTR has been interpreted as the edge of a portion of the South American plate flexured and uplifted along the transform (Fig. 1b). The VTR is believed to be generated by a one-stage short tectonic event correlated with a trans-tensive adjustment of plate motion that occurred between ~10 and 12 Ma (Bonatti *et al.*, 2006). This event caused the edge of the plate to be uplifted and tilted southward so that the uppermost crustal layer is exposed on the southern scarp of the VTR, whereas the northern scarp, acting as a footwall, exposes a section with crustal and upper mantle units (Fig. 1b). The uplifted lithospheric section subsequently moved away carried by the plate drift, its eastern tip being now located ~140 km west of the ridge axis, in crust dated at ~10 Ma. The VTR exposes an ~300 km long continuous section of oceanic lithosphere (Vema Lithospheric Section or VLS), giving us a rare chance to study the variations in time of crustal and upper mantle structure and composition along a seafloor spreading flow line. During five *Nautile* dives in 1989 (Auzende *et al.*, 1989) a 'normal' sequence of oceanic lithospheric units was observed and sampled at longitude 42°42′W. The VLS crest is topped with a few hundred meters of pillow lavas and basaltic breccias. The base of this layer grades into a 800–1200 m thick dike complex. The north–south orientation of the dikes is subparallel to the ridge axis and concordant with the abyssal hill fabric south of the VTR (Auzende *et al.*, 1989; Cannat *et al.*, 1991). Moving downward the VLS presents a bench or terrace running all along the VTR. An ~500 m thick



Downloaded from http://petrology.oxfordjournals.org/ at Kainan University on March 17, 2015

gabbroic unit with coarse-grained Fe–Ti-rich gabbros crops out at and close to the terrace. The roots of the gabbroic layer reach 4000 m below sea level (b.s.l.) where upper mantle residual peridotites crop out down to the base of the VTR (~5100 m). The base of the scarp plunges beneath the flat-lying turbidites filling the transform valley.

The morphological uniformity of the VTR suggests continuity of the residual ultramafic basal layer for about 300 km along the base of the VLS. During three expeditions with the research vessels *M. Ewing* (1993), and *A. N. Strakhov* (1998, 2000) a close-spaced (5–6 km) systematic sampling of the deepest part of the VLS was carried out moving eastward and westward from the *Nautile* sites (Table 1, Fig. 1c). All sampling >4000 m depth recovered upper mantle residual ultramafic rocks confirming the continuity of the lithospheric structure all along the VLS. Orthopyroxene-free dunites were sampled at few sites (Table 1), overall representing a rare lithology (<1%). Basalts, dolerites and gabbros from the overlying crustal layers were also collected. In this paper we describe melting and refertilization processes based on the mineral chemistry of the mantle-derived ultramafic rocks sampled along the VLS.

## METHODS

Point counting under the microscope was performed to reconstruct pre-serpentinization modal compositions (Table 2). At least 1000 points were counted on standard-size thin sections. Bastitic serpentine was attributed to orthopyroxene or clinopyroxene based on texture; mesh-serpentine with associated magnetite was attributed to olivine. No corrections for serpentinization-related volume expansion were applied.

The major element chemical composition of the mantle equilibrated primary minerals olivine, orthopyroxene, clinopyroxene and spinel (Tables 3–6) was determined with a Jeol JXA 8600 at CNR-CS per la Minerogenesi e la Geochimica Applicata, Firenze University, with a Cameca-Camebax at the CAMPARIS micro analyses centre (Paris, Campus Jussieu), and a Cameca SX-100 electron probe at the American Museum of Natural History, New York, using 15 kV acceleration voltage, 10 nA and focused beam. Matrix correction was carried out according to Bence & Albee (1968). To reduce inter-laboratory analytical variations we adopted, for each probe session, the following linearization procedure: linearization of the probe based on internal standards, check of the consistency of international standards at ±2% for the major elements and ±5% for minor elements [based on the list and procedures described by Vaggelli *et al.* (1999)], then consistency of internal standard at ±5%. As internal standard we used selected micro areas of samples S1904-42 and S1905-59.

Rare earth elements (REE) in clinopyroxenes (Table 7) were analysed by secondary ion mass spectrometry (SIMS) with a Cameca IMS 4f ion microprobe, located at CNR-IGG, Pavia. Procedures have been described by Brunelli *et al.* (2003) based on Bottazzi *et al.* (1990, 1994) and Rampone *et al.* (1991).

## ROCK DESCRIPTION

Ultramafic rocks were sampled from 28 sites along the lower part of the VLS (Table 1, Fig. 1c). Based on their petrography we divided the sampled area into three main sectors.

### Sector A

Sector A spans a distance of ~200 km away from the ridge axis between dredge sites S2209 and EW 17 (Fig. 1c). Mantle rocks from this sector are spinel harzburgites and clinopyroxene-poor lherzolites (Table 1). Textural observations, mostly based on pyroxene morphology because of the complete serpentinization of olivine, show primary undeformed coarse-grained to porphyroclastic textures. Thin magmatic veins (<2 mm) are occasionally reported, cross-cutting the primary foliation; such samples have been discarded from this study. Orthopyroxene is present as large subequant grains up to 20 mm in size in the less deformed protogranular textures. Primary grain boundaries are curvilinear, with irregular, deep, embayments filled by olivine grains. Recrystallization into large subgrains (up to 5 mm) with rare, weak undulose extinction indicates a high-temperature, low-strain, history. Rocks that underwent higher strain show small orthopyroxene (± cpx ± ol) neoblasts (0·2–0·5 mm) aligned along intracrystalline kink-bands and/or mantling relic porphyroclastic grains in pressure shadows. Anhedral small (up to 0·3 mm) orthopyroxene grains sometimes appear included in clinopyroxene porphyroclasts. Clinopyroxene porphyroclasts (<3 mm) appear to be sensitive to very low stress in the ductile clinopyroxene field, as shown by the widespread occurrence of undulose extinction and variably abundant clinopyroxene neoblasts (± opx ± ol) mantling the porphyroclastic relics. Clinopyroxene never shows evidence of brittle deformation. Large spinels vary in shape from irregular lobate grains (up to 1·5 mm in size) in clinopyroxene-rich peridotites to subhedral grains in harzburgites. These grains are sometimes poikilitic enclosing small ol ± opx ± cpx grains. Graphic vermicular spinel is often associated with orthopyroxene neoblasts or at the tip of large porphyroclastic grains. Large orthopyroxene grains usually display a thin (<10 μm) regular exsolution pattern of clinopyroxene lamellae and blebs (rarely associated with spinel). Small clinopyroxene grains, frequently associated with spinel, are interstitial in the olivine matrix or aligned to form veinlets cross-cutting the now-serpentinized olivine matrix and the pyroxene

Downloaded from http://petrology.oxfordjournals.org/ at Kainan University on March 17, 2015

*Table 1: Starting and ending latitude and longitude, bathymetric depth and rock recovery for the dredge sites used in this study*

| Dredge | Recovered rocks | Start lat. | End lat. | Start long. | End long. | Depth interval (m) |
|---|---|---|---|---|---|---|
| *R.V.* Pillsbury, *cruise P7003* | | | | | | |
| AT79 (P7003-19) | Porphyroclastic peridotite 52%, gabbro 40%, basalt 4%, amphibolite | 10°46·20 | | 42°48·00 | | 4800–4000 |
| AT83 (P7003-23) | Lherzolite, amphibolite, peridotite, gabbros | 10°42·00 | | 41°37·80 | | 3800–2880 |
| *R.V.* Charcot, *cruise CH-78* | | | | | | |
| CH-78-DR10 | Porphyroclastic peridotite 60%, amphibolites 35%, gabbros and rodingite 5% | 10°41·40 | | 42°40·80 | | 4820 |
| *R.V.* M. Ewing, *cruise EW9305* | | | | | | |
| EW9305-12 | Porphyroclastic peridotite, peridotite breccia, dolerite–basaltic breccia | 10°42·30 | 10°41·90 | 42°37·40 | 42°37·40 | 5100–4750 |
| EW9305-13 | Porphyroclastic peridotite, gabbro, clay–peridotite breccia | 10°42·30 | 10°41·70 | 42°38·30 | 42°38·40 | 5050–4700 |
| EW9305-15 | Foliated peridotite, porphyroclastic peridotite, dolerite, gabbro | 10°41·60 | 10°41·30 | 42°43·40 | 42°43·50 | 4870–4500 |
| EW9305-16 | Porphyroclastic peridotite, gabbro, basalt | 10°42·10 | 10°41·60 | 42°44·50 | 42°44·60 | 5130–4750 |
| EW9305-17 | Foliated peridotite, porphyroclastic peridotite, peridotite breccia, basalt, gabbro | 10°42·00 | 10°41·20 | 42°45·50 | 42°45·50 | 5060–4560 |
| *R.V.* R. Conrad, *cruise RC2104* | | | | | | |
| RC2104-13 | sediment, basalt, gabbro, ultramafic | 10°48·50 | 10°46·40 | 41°49·40 | 41°51·50 | 4996–4846 |
| *R.V.* A. N. Strakhov, *cruise S19* | | | | | | |
| S1902 | Peridotite 80%, dunite 1%, gabbro 18%, dolerite 1% | 10°42·3 | 10°40·30 | 42°55·10 | 42°55·10 | 4800–3700 |
| S1903 | Peridotite 90%, dunite 1%, gabbro 10%, breccia 9% | 10°42·40 | 10°41·30 | 42°57·50 | 42°57·20 | 4950–4260 |
| S1904 | Peridotite 34%, dunite 1%, gabbro 60%, breccia 5% | 10°42·60 | 10°41·50 | 43°02·00 | 43°01·70 | 4900–4500 |
| S1905 | Gabbro 50%, peridotite 45%, basalt/dolerite 5% | 10°43·10 | 10°42·64 | 43°04·80 | 43°04·70 | 5050–4750 |
| S1906 | Peridotite (1 fragment) | 10°43·70 | 10°40·33 | 43°08·20 | 43°07·56 | 5100–3700 |
| S1907 | Peridotite 60%, gabbro 30%, breccia limestone 10% | 10°43·40 | 10°41·83 | 43°09·10 | 43°08·69 | 5100–4280 |
| S1908 | Amph-peridotite mylonite 90%, dolerite 10% | 10°43·40 | 10°42·50 | 43°12·00 | 43°11·70 | 5100–4650 |
| S1909 | Amph-peridotite mylonite 100% | 10°43·30 | 10°41·80 | 43°15·50 | 43°15·60 | 4900–4200 |
| S1910 | Amph-peridotite 85%, chromite 5%, breccia 10% | 10°43·90 | 10°42·20 | 43°18·30 | 43°18·20 | 5000–4500 |
| S1911 | Amph-peridotite 95%, amph-dunite 5% | 10°42·40 | 10°42·00 | 43°21·10 | 43°21·40 | 4470–3700 |
| S1912 | Myl/porph peridotite 90%, breccia 5%, gabbro 5%, limestone <1% | 10°42·70 | 10°41·60 | 43°24·10 | 43°23·40 | 4500–3700 |
| S1913 | Myl/porph peridotite 80%, limestone 20% | 10°42·50 | 10°42·30 | 43°26·50 | 43°27·30 | 4370–4100 |
| S1915 | Amph-porphyroclastic peridotite 90%, breccia, limestone 10% | 10°43·50 | 10°42·80 | 43°30·60 | 43°30·60 | 4470–4200 |
| S1920 | Dolerite and basalt 80%, breccia 13%, myl/porph peridotite 5%, gabbro 2% | 10°45·40 | 10°44·70 | 43°34·60 | 43°35·10 | 5000–4550 |
| S1923 | Porphyroclastic peridotite 70%, gabbro 20%, limestone breccia 10% | 10°42·20 | 10°41·20 | 42°34·50 | 42°35·65 | 5200–4000 |
| S1924 | Porphyroclastic peridotite 98%, gabbro 1%, limestone 1% | 10°42·90 | 10°42·80 | 42°31·80 | 42°31·80 | 4960–4900 |
| S1925 | Porphyroclastic peridotite 80%, gabbro 14%, breccia 4%, ophicalcite 1%, limestone 1% | 10°42·60 | 10°42·50 | 42°28·60 | 42°27·80 | 5150–4850 |
| S1927 | Porphyroclastic peridotite 100% | 10°42·60 | 10°41·90 | 42°26·00 | 42°26·20 | 5000–4500 |
| S1928 | Porphyroclastic peridotite 95%, gabbro 2%, dolerite 2%, breccia 1% | 10°42·78 | 10°41·90 | 42°23·00 | 42°22·90 | 5120–4530 |
| S1930 | Porphyroclastic peridotite 98%, dunite <1%, gabbro 1%, breccia and limestone 1%, dolerite <1% | 10°40·30 | 10°39·30 | 42°08·10 | 42°08·20 | 3950–3480 |
| *R.V.* A. N. Strakhov, *cruise S22* | | | | | | |
| S2209 | Porphyroclastic peridotite 100% | 10°42·41 | 10°42·15 | 41°26·39 | 41°26·51 | 4850–4650 |
| S2218 | Peridotite, gabbro, basalt | 10°43·50 | 10°43·60 | 41°52·01 | 41°52·20 | 5200–5070 |
| S2220 | Porphyroclastic peridotite 100% | 10°42·40 | 10°41·46 | 41°57·08 | 41°57·09 | 4860–4173 |
| S2221 | Peridotite, dunite, gabbro, basalt, breccia | 10°34·04 | 10°42·60 | 42°03·72 | 42°03·03 | 4900–4800 |
| Nautile dives, VExx: refer to Auzende *et al.*, 1989 | | | | | | |

Downloaded from http://petrology.oxfordjournals.org/ at Kainan University on March 17, 2015

*Table 2: Modal mineralogy of selected peridotites from the Vema Lithospheric Section*

| | olivine | opx | cpx | sp |
|---|---|---|---|---|
| S1902-05 | 77·8 | 19·0 | 2·3 | 0·9 |
| S1902-07 | 67·5 | 27·9 | 3·2 | 1·3 |
| S1903-03 | 77·8 | 20·3 | 1·3 | 0·5 |
| S1904-38A | 70·9 | 25·1 | 1·5 | 2·1 |
| S1904-39 | 64·7 | 31·5 | 3·2 | 0·5 |
| S1904-40A | 75·6 | 21·5 | 1·1 | 1·6 |
| S1904-42A | 64·5 | 29·6 | 3·7 | 2·1 |
| S1905-56 | 70·1 | 25·6 | 2·4 | 1·9 |
| S1905-59 | 53·2 | 33·2 | 11·2 | 2·2 |
| S1912-04A | 53·7 | 28·8 | 13·2 | 4·1 |
| S1912-06 | 68·4 | 24·9 | 4·6 | 1·8 |
| S1913-01 | 71·6 | 20·4 | 5·5 | 2·3 |
| S1913-07A | 60·0 | 29·5 | 7·0 | 3·3 |
| S1923-38A | 74·7 | 23·3 | — | 1·8 |
| S1923-42A | 78·1 | 19·1 | 0·2 | 2·4 |
| S1923-84A | 76·3 | 19·5 | 2·3 | 1·7 |
| S1923-86A | 74·5 | 20·6 | 1·2 | 3·6 |
| S1924-01A | 75·8 | 14·6 | 7·4 | 2·0 |
| S1924-04 | 62·8 | 32·0 | 3·6 | 1·4 |
| S1924-12 | 75·2 | 15·7 | 4·6 | 4·3 |
| S1927-03A | 73·4 | 20·0 | 4·8 | 1·6 |
| S1927-05A | 70·6 | 23·8 | 3·1 | 2·2 |
| S1928-09A | 54·3 | 36·0 | 6·5 | 2·9 |
| S1928-10 | 63·3 | 31·4 | 2·8 | 3·1 |
| S1928-15A | 61·8 | 29·7 | 5·2 | 3·0 |
| S1928-19 | 67·9 | 25·4 | 3·7 | 2·9 |
| S1930-15A | 73·9 | 24·8 | 0·2 | 0·8 |
| S2209-01A | 78·4 | 16·3 | 4·8 | 0·5 |
| S2220-04 | 75·8 | 22·8 | 0·6 | 0·8 |
| S2220-06 | 79·8 | 18·6 | 1·3 | 0·3 |
| S2221-01A | 60·6 | 31·5 | 6·4 | 1·6 |
| S2221-04B | 75·5 | 19·9 | 3·0 | 1·6 |
| S2221-05B | 75·0 | 21·5 | 2·3 | 1·2 |
| P7003-23A | 85·8 | 12·0 | 1·1 | 1·1 |

*Table 3: Average major element oxide composition of VTR olivines*

| Sample: | S2220-04 | S2220-06 |
|---|---|---|
| *n*: | 6 | 5 |
| $SiO_2$ | 41·11(32) | 40·92(24) |
| FeO | 8·58(20) | 9·02(9) |
| MnO | 0·14(5) | 0·14(4) |
| MgO | 50·14(56) | 49·89(24) |
| CaO | 0·03(3) | 0·06(2) |
| NiO | 0·38 | — |
| Total | 100·06(61) | 100·11(34) |
| Mg-no. | 91·24(24) | 90·79(11) |

*n*, number of analyses; 1σ standard deviation in parentheses refers to the last digit.

porphyroclasts; they are evenly distributed, forming about 1–2 vol. % of the rocks on average, although they are more concentrated in a few samples and/or sites. Similar blebs and interstitial grains have been interpreted as the result of crystallization of unextracted melts (Seyler *et al.*, 2001).

## Sector B

Sector B extends from longitude 42°55′ to 43°21′W (~70 km between dredge sites S1902 and S1911, Fig. 1). It is characterized by the presence of amphibole-bearing ultramafics that we interpret as resulting from strain-free hydration of former residual peridotites. Amphibole mylonites are the prevalent lithology from sites S1907 to S1909.

## Sector C

Sector C represents the westernmost sampled area from longitude 43°24′ to 43°35′W (~25 km between dredge sites S1912 and S1920, Fig. 1). Locally abundant, highly strained, mylonitic peridotites were recovered at these sites together with less deformed porphyroclastic samples. Site S1915 in this area is dominated by amphibole-bearing porphyroclastic peridotites. Pseudomorphic serpentine, plus clay minerals and Fe-hydroxide, replace the olivine matrix, giving these rocks a typical reddish earthy appearance. Orthopyroxene is undeformed or strained with undulose extinction, sometimes cut by sinusoidal kink bands. Grains are variably elongated with aspect ratios ranging from subequant to >10:1. The large pyroxene relics are mantled by new grains of opx ± cpx (± ol; ± sp; ± pl; ± amph), which define strain shadows and sigma structures. Primary clinopyroxene, present in these samples, never records brittle deformation. Clinopyroxene porphyroclasts are usually mantled by a thick layer of cpx ± opx ± ol neoblasts sometimes completely replacing the former crystal. Spinel has a rounded, occasionally cataclastic, habit, suggesting that it was broken and rotated in the olivine matrix without significant dynamic recrystallization.

Small spinel neoblasts mark the mylonitic mineral lineation along with the pyroxene elongation. Porphyroclastic spinels are occasionally rimmed by plagioclase or its alteration products, indicating that deformation continued in the plagioclase stability field (Cannat & Seyler, 1995). Yellow–pale brownish pargasitic amphibole



Downloaded from http://petrology.oxfordjournals.org/ at Kainan University on March 17, 2015

*Table 4: Average major element oxide composition of VTR orthopyroxenes*

| Sample | *n* | $SiO_2$ | $TiO_2$ | $Al_2O_3$ | $Cr_2O_3$ | FeO | MnO | MgO | CaO | $Na_2O$ | NiO | Total | Mg-no. |
|---|---|---|---|---|---|---|---|---|---|---|---|---|---|
| S1902-05 | 3 | 55·14(9) | 0·04(3) | 4·26(31) | 0·91(2) | 6·05(9) | 0·14(4) | 33·11(53) | 1·16(32) | 0·03(3) | 0·10 | 100·87(47) | 90·69(1) |
| S1902-07 | 6 | 54·74(53) | 0·06(2) | 4·53(36) | 0·99(8) | 5·84(23) | 0·13(1) | 32·71(63) | 1·10(60) | 0·03(2) | 0·11(4) | 100·23(91) | 90·90(22) |
| S1902-23 | 5 | 54·60(39) | 0·04(2) | 5·08(38) | 0·89(11) | 6·14(14) | 0·12(2) | 32·52(67) | 0·96(96) | 0·03(3) | 0·10(4) | 100·43(92) | 90·42(12) |
| S1903-03 | 5 | 55·22(47) | 0·05(3) | 4·13(29) | 0·93(11) | 6·34(19) | 0·11(4) | 33·10(28) | 0·87(24) | 0·04(2) | 0·05(2) | 100·80(65) | 90·29(28) |
| S1903-05 | 5 | 54·47(59) | 0·04(3) | 4·93(35) | 0·81(11) | 6·36(10) | 0·15(3) | 33·19(46) | 0·99(49) | 0·04(5) | — | 100·97(54) | 90·29(6) |
| S1904-33 | 3 | 54·24(39) | 0·04(1) | 4·22(8) | 0·96(2) | 6·36(7) | 0·12(3) | 31·85(15) | 1·68(18) | 0·16(28) | 0·09(1) | 99·73(28) | 89·92(8) |
| S1904-38 | 4 | 54·30(43) | 0·04(3) | 4·33(13) | 0·83(4) | 6·07(12) | 0·14(2) | 32·25(51) | 1·24(48) | 0·00(0) | 0·11(2) | 99·26(92) | 90·45(19) |
| S1904-39 | 6 | 54·90(17) | 0·08(2) | 4·32(19) | 0·81(4) | 6·18(12) | 0·16(3) | 33·44(26) | 0·76(18) | 0·02(4) | 0·10(3) | 100·71(45) | 90·60(12) |
| S1904-40 | 4 | 55·07(27) | 0·05(1) | 4·40(7) | 1·03(6) | 5·77(12) | 0·12(2) | 32·79(33) | 1·01(65) | 0·01(2) | 0·11(2) | 100·34(54) | 91·01(9) |
| S1904-42 | 7 | 53·98(91) | 0·04(2) | 4·64(48) | 0·89(10) | 6·12(14) | 0·15(1) | 32·64(42) | 1·33(65) | 0·03(3) | 0·09(3) | 99·87(62) | 90·48(19) |
| S1905-56 | 7 | 56·23(31) | 0·03(1) | 3·58(9) | 0·84(7) | 5·84(16) | 0·12(1) | 33·27(64) | 1·19(53) | 0·02(2) | 0·12(3) | 101·17(52) | 91·04(17) |
| S1905-59 | 11 | 54·96(55) | 0·06(2) | 4·48(47) | 0·94(11) | 6·30(19) | 0·13(3) | 32·10(70) | 1·43(93) | 0·01(1) | 0·12(6) | 100·53(62) | 90·08(31) |
| S1912-04 | 6 | 54·90(89) | 0·07(3) | 5·24(82) | 0·80(18) | 6·10(27) | 0·13(1) | 32·57(82) | 1·20(45) | 0·03(3) | — | 101·04(66) | 90·48(40) |
| S1912-05 | 5 | 53·89(37) | 0·07(3) | 5·28(15) | 0·77(3) | 6·56(10) | 0·15(3) | 31·76(39) | 1·58(28) | 0·02(2) | 0·11(2) | 100·13(46) | 89·62(13) |
| S1912-06 | 4 | 54·63(45) | 0·07(2) | 5·62(12) | 0·88(4) | 6·20(11) | 0·14(2) | 31·92(33) | 1·20(39) | 0·02(2) | 0·11(0) | 100·72(61) | 90·17(14) |
| S1912-08 | 4 | 53·48(86) | 0·07(3) | 4·94(16) | 0·78(3) | 6·29(9) | 0·15(3) | 32·32(49) | 1·23(52) | 0·01(2) | 0·11(2) | 99·40(70) | 90·15(16) |
| S1912-12 | 4 | 54·50(47) | 0·08(3) | 5·57(85) | 0·79(21) | 6·32(30) | 0·14(2) | 32·72(66) | 1·38(49) | 0·05(4) | — | 101·54(60) | 90·23(33) |
| S1913-01 | 4 | 54·70(47) | 0·08(1) | 5·51(41) | 0·84(9) | 6·04(20) | 0·16(2) | 32·32(48) | 1·07(32) | 0·06(4) | 0·12(6) | 100·82(32) | 90·51(25) |
| S1913-03 | 2 | 52·95(57) | 0·15(1) | 5·94(10) | 0·95(2) | 5·91(15) | 0·11(4) | 30·74(13) | 2·60(20) | 0·09 | 0·10(0) | 99·73(31) | 90·27(18) |
| S1913-07 | 7 | 54·06(69) | 0·10(4) | 5·39(68) | 0·72(13) | 6·18(23) | 0·13(3) | 31·85(49) | 1·62(57) | 0·03(3) | 0·15(1) | 100·13(53) | 90·19(25) |
| S1913-28 | 4 | 54·59(30) | 0·06(4) | 5·32(38) | 0·84(13) | 6·08(5) | 0·12(2) | 32·90(44) | 0·63(9) | 0·05(1) | 0·12(1) | 100·68(80) | 90·60(7) |
| S1913-36 | 9 | 54·51(39) | 0·08(4) | 5·17(47) | 0·88(11) | 5·80(14) | 0·12(2) | 32·00(62) | 1·57(56) | 0·06(4) | 0·10(1) | 100·30(38) | 90·77(12) |
| S1920-84 | 3 | 54·76(65) | 0·06(3) | 5·44(36) | 0·66(8) | 6·35(24) | 0·13(3) | 32·42(57) | 1·13(17) | 0·06(4) | 0·08(1) | 101·07(71) | 90·10(40) |
| S1920-85 | 5 | 54·90(33) | 0·09(3) | 5·31(28) | 0·60(9) | 6·41(24) | 0·12(8) | 31·87(54) | 1·45(65) | 0·07(3) | — | 100·83(52) | 89·86(24) |
| S1920-88 | 4 | 54·82(48) | 0·05(3) | 5·19(39) | 0·62(3) | 6·30(8) | 0·15(5) | 32·27(28) | 1·19(18) | 0·02(3) | 0·11(1) | 100·64(58) | 90·12(10) |
| S1923-38 | 4 | 54·55(29) | 0·05(4) | 4·57(15) | 0·90(3) | 6·24(24) | 0·16(3) | 32·41(34) | 1·09(24) | 0·03(4) | 0·09(6) | 100·04(64) | 90·25(27) |
| S1923-42 | 4 | 55·23(39) | 0·07(2) | 4·42(40) | 0·86(10) | 6·03(11) | 0·15(2) | 32·58(73) | 1·08(60) | 0·01(1) | 0·08 | 100·45(47) | 90·58(30) |
| S1923-45 | 2 | 53·74(27) | 0·05(0) | 4·44(6) | 0·87(0) | 5·91(15) | 0·13(2) | 31·49(35) | 1·99(15) | 0·04(2) | 0·08(2) | 98·73(70) | 90·47(12) |
| S1923-46 | 4 | 54·46(25) | 0·05(2) | 4·94(28) | 0·93(2) | 6·36(11) | 0·15(2) | 32·79(31) | 0·70(9) | 0·05(3) | 0·08(4) | 100·50(17) | 90·19(23) |
| S1923-84 | 6 | 54·83(3) | 0·04(2) | 4·41(12) | 0·86(7) | 6·12(18) | 0·16(3) | 33·22(23) | 0·99(25) | 0·01(2) | 0·07(2) | 100·68(30) | 90·64(26) |
| S1923-86 | 5 | 54·88(37) | 0·03(0) | 4·23(40) | 0·85(15) | 6·50(21) | 0·15(2) | 32·71(38) | 1·00(47) | 0·00(0) | 0·08(5) | 100·41(71) | 89·96(30) |
| S1924-01 | 2 | 55·22(19) | 0·05(1) | 4·96(13) | 0·66(5) | 6·18(5) | 0·17(0) | 33·27(30) | 0·65(14) | 0·00(0) | — | 101·14(21) | 90·57(14) |
| S1924-03 | 7 | 54·72(49) | 0·08(2) | 5·18(42) | 0·63(11) | 6·47(21) | 0·16(4) | 32·57(43) | 1·33(13) | 0·04(3) | — | 101·16(49) | 89·98(29) |
| S1924-04 | 1 | 54·99 | 0·12 | 5·55 | 0·79 | 6·43 | 0·08 | 32·12 | 1·01 | 0·06 | — | 101·15 | 89·90 |
| S1924-05 | 4 | 53·90(29) | 0·08(1) | 5·73(20) | 0·85(5) | 6·31(23) | 0·16(2) | 32·14(59) | 1·00(46) | 0·01(3) | 0·15(1) | 100·26(41) | 90·08(31) |
| S1924-12 | 4 | 54·08(43) | 0·06(2) | 5·81(26) | 0·73(3) | 6·60(19) | 0·16(2) | 32·25(23) | 0·62(14) | 0·02(2) | 0·11(5) | 100·40(39) | 89·69(32) |
| S1925-05 | 7 | 54·70(43) | 0·08(1) | 5·34(36) | 0·72(9) | 6·42(22) | 0·15(4) | 32·36(28) | 0·81(37) | 0·02(2) | 0·09(2) | 100·64(61) | 89·99(24) |
| S1925-56 | | 54·68(36) | 0·07(3) | 4·44(26) | 0·85(4) | 6·47(17) | 0·12(4) | 32·26(44) | 0·66(26) | 0·01(1) | 0·10(2) | 99·66(47) | 89·88(30) |
| S1925-71 | 12 | 54·59(43) | 0·06(3) | 4·45(22) | 0·83(5) | 6·16(10) | 0·14(4) | 32·34(49) | 1·56(26) | 0·02(2) | 0·09(2) | 100·26(51) | 90·34(13) |
| S1925-77 | 3 | 54·54(23) | 0·07(1) | 4·85(24) | 0·93(10) | 5·97(14) | 0·12(1) | 33·01(35) | 1·07(71) | 0·01(0) | — | 100·85(82) | 90·78(16) |
| S1927-01 | 4 | 54·30(47) | 0·04(1) | 4·57(36) | 0·91(8) | 6·23(19) | 0·13(4) | 32·24(96) | 1·46(82) | 0·01(2) | 0·11(5) | 99·97(70) | 90·21(4) |
| S1927-02 | 4 | 55·10(22) | 0·03(4) | 4·61(48) | 0·88(66) | 6·16(17) | 0·12(4) | 32·19(40) | 1·06(32) | 0·01(2) | 0·09(3) | 99·95(47) | 90·30(23) |
| S1927-03 | 4 | 55·01(58) | 0·03(3) | 4·83(22) | 0·93(7) | 6·43(16) | 0·14(3) | 32·61(25) | 0·79(18) | 0·02(1) | 0·10(2) | 100·81(65) | 90·05(21) |
| S1927-05 | 5 | 54·42(38) | 0·04(2) | 4·64(15) | 0·90(10) | 6·41(24) | 0·13(4) | 32·75(25) | 0·72(3) | 0·01(2) | 0·14(13) | 100·38(50) | 90·10(39) |
| S1928-09 | 5 | 54·60(40) | 0·06(4) | 4·71(24) | 0·85(7) | 6·21(11) | 0·12(2) | 32·36(55) | 1·17(18) | 0·02(3) | 0·06(2) | 100·32(88) | 90·28(21) |
| S1928-10 | 4 | 54·51(61) | 0·07(2) | 5·00(12) | 0·88(4) | 5·99(3) | 0·12(3) | 32·58(50) | 1·10(9) | 0·01(2) | 0·10(1) | 100·33(92) | 90·65(13) |
| S1928-13 | 8 | 55·01(19) | 0·05(2) | 4·37(33) | 0·83(11) | 6·18(24) | 0·08(5) | 32·86(43) | 1·23(32) | 0·01(1) | 0·10(5) | 100·73(52) | 90·45(38) |
| S1928-14 | 5 | 54·86(26) | 0·08(4) | 4·87(24) | 0·79(13) | 6·19(30) | 0·15(8) | 32·40(61) | 1·24(50) | 0·02(2) | 0·06(6) | 100·68(41) | 90·31(48) |

Downloaded from http://petrology.oxfordjournals.org/ at Kainan University on March 17, 2015

| Sample | *n* | $SiO_2$ | $TiO_2$ | $Al_2O_3$ | $Cr_2O_3$ | FeO | MnO | MgO | CaO | $Na_2O$ | NiO | Total | Mg-no. |
|---|---|---|---|---|---|---|---|---|---|---|---|---|---|
| S1928-15 | 22 | 54·69(49) | 0·06(3) | 4·73(46) | 0·77(14) | 6·20(24) | 0·12(5) | 32·52(48) | 1·14(34) | 0·02(2) | 0·09(6) | 100·32(76) | 90·34(39) |
| S1928-19 | 3 | 54·92(36) | 0·06(6) | 4·79(25) | 0·92(6) | 6·17(12) | 0·13(4) | 32·51(21) | 1·11(23) | 0·03(5) | 0·09 | 100·67(36) | 90·37(22) |
| S1930-70 | 1 | 55·74 | 0·05 | 3·44 | 0·87 | 5·63 | 0·12 | 33·17 | 1·26 | 0·00 | — | 100·28 | 91·30 |
| S1930-79 | 4 | 54·99(37) | 0·04(1) | 3·63(5) | 0·98(3) | 6·02(31) | 0·11(5) | 32·83(34) | 1·40(6) | 0·02(3) | 0·12(3) | 100·10(44) | 90·67(48) |
| S1930-134 | 4 | 56·01(28) | 0·04(1) | 3·12(14) | 0·72(12) | 6·43(28) | 0·17(1) | 32·65(44) | 1·35(59) | 0·01(2) | 0·10(3) | 100·60(37) | 90·05(34) |
| S2209-01 | 3 | 54·35(12) | 0·05(3) | 3·70(10) | 0·85(2) | 6·15(23) | 0·09(2) | 32·72(39) | 1·89(38) | 0·03(2) | 0·11(5) | 99·95(50) | 90·46(22) |
| S2220-04 | 7 | 55·19(40) | 0·03(2) | 4·21(19) | 0·78(5) | 5·98(15) | 0·16(3) | 32·71(27) | 1·49(32) | 0·03(3) | — | 100·58(68) | 90·69(20) |
| S2220-06 | 3 | 55·30(68) | 0·05(2) | 4·09(15) | 0·90(7) | 6·13(12) | 0·13(5) | 32·72(15) | 1·20(18) | 0·02(3) | 0·07(1) | 100·58(47) | 90·49(21) |
| S2221-01 | 8 | 54·51(23) | 0·03(2) | 4·30(27) | 0·87(8) | 6·12(11) | 0·09(4) | 33·09(22) | 0·81(8) | 0·01(1) | 0·12(1) | 99·93(25) | 90·60(16) |
| S2221-04 | 7 | 54·29(38) | 0·06(2) | 4·88(19) | 0·99(6) | 6·38(15) | 0·14(3) | 32·90(53) | 0·87(23) | 0·02(2) | 0·07(3) | 100·57(44) | 90·19(27) |
| S2221-05 | 4 | 54·54(46) | 0·05(2) | 4·61(9) | 0·95(6) | 6·12(12) | 0·17(2) | 32·72(13) | 1·21(8) | 0·01(3) | 0·10(1) | 100·45(46) | 90·49(19) |
| VE1-1 | 4 | 54·45(48) | 0·05(5) | 5·13(62) | 0·86(11) | 6·28(19) | 0·19(3) | 32·28(42) | 1·02(37) | 0·03(3) | 0·09(1) | 100·33(64) | 90·15(36) |
| VE1-2 | 3 | 54·63(31) | 0·06(2) | 5·23(39) | 0·92(2) | 6·41(20) | 0·14(3) | 32·16(67) | 0·96(85) | 0·01(1) | — | 100·52(13) | 89·95(13) |
| VE1-3 | 4 | 54·97(22) | 0·06(1) | 4·74(20) | 0·74(7) | 6·05(29) | 0·13(2) | 32·01(63) | 1·30(71) | 0·02(3) | 0·09(2) | 100·11(11) | 90·41(26) |
| VE1-5 | 5 | 54·43(40) | 0·06(3) | 4·85(39) | 0·86(10) | 6·38(22) | 0·12(2) | 32·35(39) | 1·21(43) | 0·02(4) | 0·09 | 100·33(66) | 90·03(25) |
| VE1-7 | 3 | 54·72(29) | 0·06(2) | 4·71(15) | 0·94(6) | 6·37(8) | 0·12(2) | 32·42(51) | 0·83(51) | 0·02(2) | 0·11(1) | 100·32(29) | 90·07(10) |
| VE 4-4 | 2 | 54·84(13) | 0·06(1) | 3·99(4) | 0·85(1) | 6·42(24) | 0·16(5) | 33·71(43) | 0·88(43) | 0·04(2) | | 100·95(22) | 90·34(22) |
| VE 4-7 | 4 | 54·27(38) | 0·05(2) | 4·78(22) | 0·90(3) | 6·15(30) | 0·12(2) | 32·77(86) | 1·13(95) | 0·01(1) | 0·09(1) | 100·24(33) | 90·48(35) |
| P7003-19-J | 4 | 54·00(45) | 0·03(1) | 4·24(21) | 0·97(8) | 5·72(11) | 0·11(1) | 32·90(94) | 1·16(71) | 0·01(2) | 0·10(1) | 99·23(85) | 91·11(23) |
| P7003-23-A | 6 | 55·26(51) | 0·03(1) | 3·64(19) | 0·97(16) | 6·02(13) | 0·13(1) | 33·12(28) | 1·22(25) | 0·02(2) | — | 100·42(38) | 90·74(20) |
| CH78 DR10-1 | 3 | 54·70(86) | 0·08(2) | 3·96(19) | 0·73(6) | 6·13(8) | 0·11(2) | 33·02(54) | 1·46(59) | 0·02(2) | 0·07(3) | 100·28(83) | 90·56(11) |
| EW12-5 | 5 | 55·29(70) | 0·05(1) | 4·96(33) | 0·76(7) | 6·21(15) | 0·10(5) | 32·57(47) | 0·84(70) | 0·00(0) | 0·08(1) | 100·83(131) | 90·33(21) |
| EW13-3 | 7 | 54·78(25) | 0·04(2) | 4·38(30) | 0·76(14) | 6·30(32) | 0·07(6) | 32·99(55) | 0·95(53) | 0·04(4) | 0·05(4) | 100·33(62) | 90·31(54) |
| EW13-7 | 10 | 54·38(22) | 0·05(3) | 4·67(18) | 0·86(11) | 6·22(17) | 0·08(6) | 32·90(37) | 1·02(51) | 0·02(3) | — | 100·20(45) | 90·41(32) |
| EW 15-7 | 4 | 54·41(36) | 0·07(4) | 5·04(19) | 0·67(8) | 6·90(23) | 0·15(2) | 32·11(54) | 0·73(35) | 0·03(3) | — | 100·12(48) | 89·23(38) |
| EW16-1 | 7 | 55·50(73) | 0·03(2) | 4·54(36) | 0·91(3) | 6·02(16) | 0·11(4) | 32·41(58) | 1·05(55) | 0·02(3) | — | 100·59(59) | 90·56(27) |
| EW16-5 | 3 | 54·01(47) | 0·07(1) | 4·62(25) | 0·88(12) | 6·27(3) | 0·15(3) | 33·66(50) | 0·68(20) | 0·02(2) | — | 100·37(82) | 90·54(9) |
| EW16-6 | 6 | 54·89(46) | 0·05(3) | 4·37(44) | 0·74(21) | 6·33(21) | 0·12(2) | 33·28(46) | 0·81(45) | 0·02(2) | — | 100·60(83) | 90·36(31) |
| EW16-7 | 7 | 54·99(38) | 0·06(3) | 4·54(38) | 0·93(9) | 6·06(33) | 0·13(2) | 33·06(52) | 1·09(43) | 0·02(2) | — | 100·88(74) | 90·68(43) |
| EW17-3 | 6 | 54·36(26) | 0·07(3) | 4·69(20) | 0·85(13) | 6·14(15) | 0·09(7) | 32·68(68) | 1·12(94) | 0·02(2) | — | 100·01(83) | 90·47(12) |
| RC21-13AC | 6 | 55·23(71) | 0·02(2) | 3·27(12) | 0·75(4) | 5·95(28) | 0·15(3) | 33·18(39) | 1·79(21) | 0·02(3) | 0·12(4) | 100·45(100) | 90·86(36) |

*n*, number of analyses; 1σ standard deviation in parentheses refers to the last digit.

appears in few samples associated with the neoblastic paragenesis (site S1915). We excluded from this study all plagioclase- and amphibole-bearing samples, taking into account only the more primary textures equilibrated in the spinel stability field. Because serpentinization and weathering make it difficult to recognize the presence of plagioclase, we used only samples with <0·15% $TiO_2$ in spinel. This threshold in $TiO_2$ content helps in recognizing the former presence of small amounts of plagioclase and cryptic metasomatic events caused by low-*P* rock reactions with high-Ti melts (Dick and Bullen, 1984; Seyler and Bonatti, 1997).

## MINERAL CHEMISTRY

All VLS peridotites have undergone high degrees of serpentinization and weathering (≥80%), with fresh olivine observed in only two samples: S2220-04 and 06 (Fo 91·2 and 90·8, respectively; NiO 0·38 wt %, Table 3). Major element compositions of the other relic phases (pyroxenes and spinel) in the peridotites from sectors A and C (Tables 3–6) range within the field of normal residual abyssal peridotites (Dick & Bullen, 1984; Michael & Bonatti, 1985; Dick, 1989; Bonatti *et al.*, 1993; Ghose *et al.*, 1996; Hellebrand *et al.*, 2002; Brunelli *et al.*, 2003; Seyler *et al.*, 2003).

### Spinel

Spinel Cr-number [=100 × Cr/(Cr + Al)] ranges from 13·0 (sample S1920-84) to 37·4 (sample S1930-70) within the abyssal peridotite field (see references above). Spinel Cr-number shows a good correlation with the Mg-number [100 × Mg/(Mg + Fe); all Fe as $Fe^{2+}$] of associated orthopyroxene, but a weak and dispersed correlation

Downloaded from http://petrology.oxfordjournals.org/ at Kainan University on March 17, 2015

*Table 5: Average major element oxide composition of VTR clinopyroxenes*

| Sample | *n* | $SiO_2$ | $TiO_2$ | $Al_2O_3$ | $Cr_2O_3$ | FeO | MnO | MgO | CaO | $Na_2O$ | NiO | Total | Mg-no. |
|---|---|---|---|---|---|---|---|---|---|---|---|---|---|
| S1902-05 | 8 | 51·45(35) | 0·10(3) | 5·21(61) | 1·32(20) | 2·58(26) | 0·07(2) | 16·46(41) | 23·01(84) | 0·18(12) | 0·04(3) | 100·40(43) | 91·93(66) |
| S1902-07 | 5 | 51·49(55) | 0·15(2) | 5·11(51) | 1·36(16) | 2·17(10) | 0·08(2) | 15·73(37) | 23·01(44) | 0·40(4) | 0·05(4) | 99·56(47) | 92·81(30) |
| S1902-23 | 4 | 50·94(23) | 0·15(1) | 6·10(45) | 1·22(13) | 2·23(17) | 0·09(5) | 15·23(19) | 23·76(19) | 0·24(2) | 0·04(2) | 99·99(54) | 92·41(59) |
| S1903-03 | 3 | 51·62(30) | 0·13(5) | 5·24(22) | 1·35(2) | 2·21(4) | 0·09(2) | 16·03(9) | 23·48(31) | 0·26(4) | — | 100·41(66) | 92·82(10) |
| S1903-05 | 1 | 50·31 | 0·18 | 6·28 | 1·19 | 2·36 | 0·07 | 15·41 | 23·52 | 0·20 | — | 99·52 | 92·09 |
| S1904-33 | 4 | 51·02(54) | 0·13(4) | 5·10(14) | 1·35(4) | 2·49(16) | 0·07(2) | 16·29(21) | 23·36(55) | 0·11(3) | 0·05(4) | 99·97(68) | 92·11(43) |
| S1904-38 | 4 | 51·13(26) | 0·12(1) | 5·19(42) | 1·31(9) | 2·45(36) | 0·07(1) | 16·32(67) | 22·68(66) | 0·18(6) | 0·07(1) | 99·48(71) | 92·26(74) |
| S1904-39 | 5 | 51·10(23) | 0·15(2) | 5·23(16) | 1·23(2) | 2·39(16) | 0·09(3) | 16·14(36) | 23·05(47) | 0·33(4) | 0·04(2) | 99·73(39) | 92·32(44) |
| S1904-40 | 5 | 51·62(31) | 0·10(2) | 4·84(30) | 1·48(7) | 2·06(8) | 0·08(3) | 16·29(55) | 23·42(27) | 0·25(3) | 0·05(2) | 100·20(44) | 93·36(24) |
| S1904-42 | 2 | 51·06(38) | 0·11(3) | 5·79(44) | 1·38(15) | 2·36(24) | 0·10(3) | 15·96(40) | 23·20(99) | 0·35(4) | — | 100·33(10) | 92·34(55) |
| S1905-56 | 5 | 51·41(38) | 0·08(2) | 5·32(99) | 1·36(12) | 2·33(10) | 0·08(2) | 15·99(25) | 23·52(31) | 0·10(3) | 0·09(1) | 100·24(39) | 92·44(35) |
| S1905-59 | 12 | 51·39(28) | 0·12(2) | 5·12(40) | 1·36(14) | 2·43(25) | 0·08(4) | 15·97(33) | 23·60(64) | 0·08(2) | 0·03(2) | 100·16(61) | 92·14(67) |
| S1912-04 | 10 | 51·34(55) | 0·22(3) | 6·24(58) | 1·30(9) | 2·85(24) | 0·08(2) | 15·95(67) | 22·16(52) | 0·49(11) | — | 100·64(61) | 90·90(55) |
| S1912-05 | 1 | 51·00 | 0·14 | 6·31 | 1·16 | 3·36 | 0·09 | 15·98 | 21·43 | 0·36 | 0·01 | 99·87 | 89·44 |
| S1912-06 | 6 | 50·97(17) | 0·19(3) | 6·59(19) | 1·20(5) | 2·76(14) | 0·11(2) | 15·37(24) | 22·69(43) | 0·42(4) | 0·06(0) | 100·33(36) | 90·84(45) |
| S1912-08 | 2 | 51·00(0) | 0·19(1) | 5·23(39) | 1·08(1) | 3·01(1) | 0·08(1) | 17·05(50) | 21·50(48) | 0·27(24) | 0·04(0) | 99·46(63) | 90·99(23) |
| S1912-12 | 6 | 50·92(39) | 0·24(6) | 6·34(36) | 1·12(10) | 2·90(21) | 0·10(4) | 15·96(51) | 22·50(59) | 0·40(3) | — | 100·47(25) | 90·76(57) |
| S1913-01 | 4 | 51·30(63) | 0·22(1) | 6·56(30) | 1·27(3) | 2·56(26) | 0·08(2) | 15·57(44) | 21·71(116) | 0·85(5) | 0·05(1) | 100·04(77) | 91·51(67) |
| S1913-03 | 1 | 51·58 | 0·29 | 5·93 | 1·13 | 2·67 | 0·07 | 15·78 | 21·56 | 0·73 | 0·00 | 99·73 | 91·32 |
| S1913-07 | 4 | 50·85(54) | 0·21(2) | 6·71(25) | 1·18(14) | 3·17(66) | 0·08(2) | 16·16(167) | 21·18(208) | 0·57(6) | 0·04(3) | 100·15(105) | 90·15(89) |
| S1913-28 | 5 | 50·86(52) | 0·25(1) | 7·15(26) | 1·32(7) | 2·81(28) | 0·11(2) | 15·42(141) | 21·31(170) | 0·79(7) | 0·09(2) | 100·08(37) | 90·72(25) |
| S1913-36 | 3 | 52·61(41) | 0·25(4) | 5·17(134) | 1·15(35) | 2·28(9) | 0·06(3) | 16·08(78) | 22·32(5) | 1·00(21) | 0·05(1) | 101·00(57) | 92·64(17) |
| S1920-84 | 5 | 51·10(66) | 0·26(3) | 6·69(76) | 0·98(17) | 2·72(34) | 0·10(3) | 15·61(30) | 22·38(95) | 0·72(7) | 0·00 | 100·55(69) | 91·10(108) |
| S1920-85 | 6 | 50·92(46) | 0·31(7) | 6·93(16) | 1·04(7) | 2·98(28) | 0·11(3) | 15·25(64) | 22·08(83) | 0·69(8) | 0·04(1) | 100·33(47) | 90·13(49) |
| S1920-88 | 4 | 50·98(46) | 0·23(5) | 6·91(13) | 1·08(11) | 2·94(8) | 0·10(4) | 15·31(23) | 21·45(53) | 0·74(7) | 0·07(4) | 99·76(23) | 90·28(32) |
| S1923-38 | 4 | 50·98(40) | 0·14(2) | 4·14(38) | 1·15(5) | 2·37(11) | 0·09(3) | 15·98(21) | 23·23(40) | 0·09(6) | 0·03(3) | 99·18(24) | 92·31(25) |
| S1923-42 | 3 | 51·36(65) | 0·18(6) | 5·63(35) | 1·36(4) | 2·37(7) | 0·07(1) | 16·03(45) | 23·65(14) | 0·16(2) | — | 100·83(86) | 92·32(39) |
| S1923-45 | 1 | 50·51 | 0·16 | 5·69 | 1·43 | 2·39 | 0·09 | 16·50 | 21·89 | 0·12 | 0·04 | 98·83 | 92·49 |
| S1923-46 | 4 | 51·68(64) | 0·12(3) | 5·41(1) | 1·44(1) | 2·49(3) | 0·10(3) | 16·12(42) | 23·31(55) | 0·05(7) | 0·05(2) | 100·81(92) | 92·01(9) |
| S1923-84 | 4 | 50·95(43) | 0·11(5) | 5·76(18) | 1·41(5) | 2·67(20) | 0·09(5) | 16·44(40) | 23·28(69) | 0·15(4) | 0·07(3) | 100·91(113) | 91·64(54) |
| S1923-86 | 4 | 50·93(32) | 0·11(2) | 5·19(14) | 1·29(5) | 2·59(12) | 0·08(2) | 16·12(53) | 22·89(67) | 0·15(4) | 0·06(3) | 99·39(29) | 91·73(20) |
| S1924-01 | 2 | 51·38(4) | 0·23(8) | 6·62(33) | 1·09(4) | 2·45(37) | 0·09(1) | 15·56(30) | 23·05(7) | 0·58(4) | — | 101·03(104) | 91·89(97) |
| S1924-03 | 3 | 50·62(62) | 0·20(5) | 6·78(22) | 1·11(6) | 3·02(25) | 0·09(2) | 15·84(47) | 21·97(43) | 0·39(3) | 0·05(1) | 100·04(78) | 90·33(46) |
| S1924-04 | 2 | 51·58(113) | 0·22(4) | 6·96(7) | 1·03(4) | 3·50(83) | 0·11(2) | 15·85(0) | 22·31(0) | 0·35(8) | — | 100·63(4) | 90·09(81) |
| S1924-05 | 4 | 50·22(16) | 0·22(3) | 6·93(14) | 1·14(5) | 2·60(10) | 0·11(1) | 14·91(21) | 22·64(30) | 0·53(7) | 0·7(1) | 99·35(37) | 91·10(28) |
| S1924-12 | 5 | 50·55(54) | 0·21(4) | 6·83(25) | 1·02(11) | 2·48(12) | 0·11(2) | 14·80(18) | 23·39(29) | 0·32(15) | 0·09(2) | 99·74(59) | 91·40(41) |
| S1925-05 | 4 | 50·74(47) | 0·24(1) | 6·89(22) | 1·13(3) | 2·54(7) | 0·08(5) | 15·12(12) | 22·71(20) | 0·50(4) | 0·04(2) | 99·99(76) | 91·37(25) |
| S1925-71 | 4 | 51·54(34) | 0·14(3) | 5·40(53) | 1·23(14) | 2·71(28) | 0·09(2) | 16·87(92) | 22·45(136) | 0·21(3) | 0·04(2) | 100·70(58) | 91·74(41) |
| S1925-77 | 5 | 49·43(32) | 0·16(3) | 6·13(26) | 1·47(5) | 2·33(10) | 0·10(3) | 15·16(14) | 23·56(13) | 0·34(2) | 0·04(2) | 98·73(17) | 92·06(38) |
| S1927-01 | 5 | 50·21(55) | 0·14(4) | 5·67(13) | 1·33(6) | 2·58(22) | 0·10(3) | 15·97(73) | 22·96(89) | 0·13(4) | 0·07(4) | 99·10(73) | 91·70(3) |
| S1927-02 | 4 | 51·07(56) | 0·13(3) | 4·65(73) | 1·12(18) | 2·33(14) | 0·08(5) | 16·26(49) | 23·30(36) | 0·12(5) | 0·02(2) | 99·09(13) | 92·55(29) |
| S1927-03 | 4 | 50·90(22) | 0·11(1) | 5·93(36) | 1·35(6) | 2·88(56) | 0·09(3) | 16·36(82) | 22·35(128) | 0·15(7) | 0·03(1) | 100·14(88) | 91·06(112) |
| S1927-05 | 9 | 51·36(28) | 0·13(4) | 5·40(15) | 1·33(4) | 2·57(25) | 0·10(7) | 16·21(54) | 23·45(83) | 0·11(1) | 0·07(9) | 100·72(47) | 91·85(57) |
| S1928-09 | 5 | 50·89(46) | 0·16(4) | 5·85(67) | 1·18(12) | 2·69(12) | 0·09(2) | 15·54(36) | 23·33(37) | 0·23(5) | 0·04(2) | 99·97(98) | 91·14(38) |
| S1928-10 | 5 | 50·74(27) | 0·18(1) | 5·91(33) | 1·27(9) | 2·71(13) | 0·12(2) | 15·35(20) | 23·02(75) | 0·24(8) | 0·07(2) | 99·57(55) | 90·98(46) |
| S1928-13 | 2 | 51·86(79) | 0·16(3) | 5·19(33) | 1·16(17) | 3·13(7) | 0·05(8) | 17·67(47) | 21·47(12) | 0·18(2) | — | 100·98(51) | 90·95(41) |
| S1928-14 | 6 | 50·59(31) | 0·14(4) | 5·89(17) | 1·25(15) | 2·66(29) | 0·10(7) | 15·81(47) | 23·05(58) | 0·18(3) | 0·06(9) | 99·73(71) | 91·39(69) |
| S1928-15 | 3 | 50·92(55) | 0·17(3) | 5·78(14) | 1·22(13) | 2·66(7) | 0·08(2) | 15·58(44) | 23·05(30) | 0·22(4) | — | 99·68(88) | 91·25(6) |
| S1928-19 | 4 | 50·86(38) | 0·14(4) | 5·78(17) | 1·27(4) | 2·63(2) | 0·11(4) | 15·75(14) | 23·36(56) | 0·18(4) | 0·03 | 100·10(22) | 91·44(8) |

Downloaded from http://petrology.oxfordjournals.org/ at Kainan University on March 17, 2015

| Sample | *n* | $SiO_2$ | $TiO_2$ | $Al_2O_3$ | $Cr_2O_3$ | FeO | MnO | MgO | CaO | $Na_2O$ | NiO | Total | Mg-no. |
|---|---|---|---|---|---|---|---|---|---|---|---|---|---|
| S1930-70 | 2 | 51·65(25) | 0·10(1) | 4·88(26) | 1·46(1) | 2·90(12) | 0·13(0) | 16·59(39) | 22·04(17) | 0·01(1) | — | 99·64(42) | 91·07(53) |
| S1930-79 | 11 | 51·14(27) | 0·07(1) | 4·69(14) | 1·49(8) | 3·05(33) | 0·10(3) | 17·33(72) | 21·98(102) | 0·03(3) | 0·05(3) | 99·90(44) | 91·04(67) |
| S1930-134 | 4 | 51·28(73) | 0·07(2) | 4·58(33) | 1·45(6) | 3·02(15) | 0·08(2) | 16·08(26) | 23·06(35) | 0·04(3) | 0·02(2) | 99·66(68) | 90·48(31) |
| S2209-01 | 4 | 50·72(32) | 0·08(2) | 4·78(15) | 1·37(8) | 2·76(3) | 0·07(5) | 16·81(20) | 22·57(11) | 0·14(1) | 0·08(4) | 99·35(49) | 91·57(5) |
| S2220-04 | 2 | 51·46(0) | 0·12(1) | 5·58(4) | 1·23(5) | 2·76(8) | 0·11(2) | 16·41(40) | 23·15(36) | 0·15(1) | | 100·95(11) | 91·37(5) |
| S2220-06 | 6 | 51·09(34) | 0·08(3) | 5·31(6) | 1·42(6) | 3·01(25) | 0·11(4) | 16·45(24) | 22·73(44) | 0·14(3) | | 100·34(34) | 90·70(64) |
| S2221-01 | 8 | 50·45(31) | 0·13(3) | 5·57(35) | 1·36(6) | 2·45(19) | 0·02(3) | 15·99(18) | 23·25(43) | 0·25(3) | 0·05(3) | 99·53(25) | 92·08(62) |
| S2221-04 | 3 | 50·87(22) | 0·14(2) | 5·70(36) | 1·40(5) | 2·85(23) | 0·11(4) | 16·13(15) | 23·03(25) | 0·26(2) | 0·08 | 100·51(72) | 90·97(60) |
| S2221-05 | 3 | 50·75(8) | 0·19(1) | 6·18(10) | 1·38(4) | 2·78(19) | 0·10(4) | 15·66(13) | 22·89(16) | 0·15(6) | | 100·09(4) | 90·94(53) |
| VE1-1 | 6 | 51·15(42) | 0·17(5) | 5·53(59) | 1·04(12) | 2·53(25) | 0·10(5) | 15·94(63) | 22·77(43) | 0·39(4) | 0·04(2) | 99·63(77) | 91·80(95) |
| VE1-2 | 1 | 51·03 | 0·16 | 6·49 | 1·28 | 2·56 | 0·06 | 15·51 | 23·12 | 0·34 | | 100·55 | 91·52 |
| VE1-3 | 3 | 51·14(38) | 0·19(2) | 6·47(35) | 1·17(5) | 2·54(11) | 0·09(3) | 15·22(22) | 23·00(14) | 0·33(3) | 0·07(3) | 100·22(72) | 91·45(22) |
| VE1-5 | 5 | 50·54(51) | 0·16(2) | 6·06(39) | 1·31(7) | 2·72(13) | 0·09(4) | 15·91(55) | 23·20(79) | 0·28(2) | 0·06(2) | 100·31(89) | 91·25(22) |
| VE1-7 | 4 | 50·95(18) | 0·15(1) | 5·77(16) | 1·24(5) | 2·40(20) | 0·09(2) | 15·45(28) | 23·25(33) | 0·21(2) | | 99·55(25) | 91·98(65) |
| VE 4-4 | 1 | 51·44 | 0·12 | 5·07 | 1·49 | 2·14 | 0·07 | 16·20 | 23·21 | 0·32 | | 100·06 | 93·10 |
| VE 4-7 | 4 | 50·96(47) | 0·15(2) | 5·63(8) | 1·32(5) | 2·44(9) | 0·07(4) | 15·99(17) | 23·11(74) | 0·16(5) | 0·05(3) | 99·86(67) | 92·10(34) |
| P7003-19-J | 3 | 50·95(42) | 0·17(1) | 5·13(12) | 1·35(7) | 2·14(20) | 0·08(1) | 16·56(99) | 23·42(125) | 0·20(4) | 0·04(4) | 100·03(63) | 93·23(36) |
| P7003-23-A | 5 | 52·10(65) | 0·07(3) | 4·50(36) | 1·36(17) | 2·67(36) | 0·08(2) | 17·13(58) | 22·51(68) | 0·02(2) | — | 100·46(67) | 91·97(82) |
| CH78 DR10-1 | 3 | 50·17(34) | 0·19(2) | 5·72(22) | 1·41(5) | 3·53(49) | 0·06(2) | 19·39(196) | 18·00(248) | 0·31(6) | — | 98·78(32) | 90·75(39) |
| EW12-5 | 4 | 52·46(36) | 0·19(2) | 4·29(43) | 0·80(18) | 2·39(18) | 0·09(2) | 16·30(20) | 23·36(26) | 0·28(2) | 0·05(4) | 100·20(46) | 92·41(56) |
| EW13-3 | 6 | 50·56(51) | 0·15(5) | 5·69(43) | 1·28(9) | 2·39(7) | 0·04(4) | 15·61(15) | 23·97(63) | 0·24(3) | 0·05(2) | 99·95(43) | 92·10(17) |
| EW16-1 | 2 | 52·10(141) | 0·17(2) | 5·23(123) | 1·19(8) | 2·22(17) | 0·10(7) | 15·87(71) | 23·10(108) | 0·33(0) | — | 100·30(168) | 92·71(82) |
| EW16-5 | 2 | 51·93(170) | 0·22(1) | 5·17(81) | 1·20(29) | 2·32(19) | 0·08(3) | 16·09(52) | 23·75(81) | 0·32(0) | — | 101·07(175) | 92·52(80) |
| EW16-6 | 5 | 51·16(60) | 0·18(3) | 5·39(48) | 1·34(8) | 2·41(35) | 0·06(3) | 15·93(66) | 22·40(90) | 0·27(3) | — | 99·15(92) | 92·20(72) |
| EW16-7 | 7 | 51·07(31) | 0·20(5) | 5·51(24) | 1·51(6) | 2·44(9) | 0·06(3) | 15·98(25) | 23·24(39) | 0·35(3) | 0·04 | 100·36(34) | 92·12(26) |
| EW17-3 | 3 | 50·59(23) | 0·20(0) | 6·79(30) | 1·41(3) | 2·34(18) | 0·06(2) | 15·22(51) | 23·12(30) | 0·33(4) | 0·05(1) | 100·10(62) | 92·07(38) |
| RC21-13AC | 5 | 51·04(94) | 0·08(1) | 4·60(18) | 1·27(5) | 2·95(24) | 0·08(1) | 17·48(30) | 22·36(90) | 0·03(2) | 0·05(4) | 99·93(120) | 91·35(56) |

*n*, number of analyses; 1σ standard deviation in parentheses refers to the last digit.

with that of associated clinopyroxene. On the other hand, the Al–Cr distribution between spinel and both pyroxenes indicates equilibration among these phases (Fig. 2a).

## Orthopyroxene

Core–rim and large-to-small orthopyroxene grain compositional variations define unique trends at the sample scale. Al, Cr and Ca decrease whereas Si and Mg increase from core to rim and from large to small grains. All other elements are weakly correlated. These variations result in a weak increase of the Mg-number and a weak decrease in Cr/Al ratio and wollastonite content from core to rim.

Figure 2 shows the compositional correlation of the Cr-number of residual spinel and clinopyroxene with orthopyroxene (sample averages). The positive Cr-number correlations are consistent with residual compositions after partial melting of a uniform source and record equilibration under mantle conditions (spinel field).

Orthopyroxene Mg-number varies from 89·6 to 91·3, decreasing with $Al_2O_3$, consistent with a partial melting trend (Tables 4–6). The ratio of olivine/orthopyroxene Mg-number of the two, fresh, olivine-bearing samples is close to unity (1·005 ± 0·002), suggesting equilibrium under high-temperature mantle conditions. Assuming equilibrium partitioning between orthopyroxene and olivine of ∼1 (Seyler *et al.*, 2003), the forsterite content of the VLS olivines is expected to range within the field of variation of abyssal peridotites.

## Clinopyroxene

Clinopyroxene major element composition displays a larger variation at the thin-section scale than that of associated orthopyroxene. Even though we selected samples with the characteristics of residual peridotites, the mineral composition dispersion appears to increase at those sites where strongly deformed amphibole-bearing rocks or contacts with gabbroic veins were also collected (sites S1902 to 05 and S1925). Positive Cr-number correlation

Downloaded from http://petrology.oxfordjournals.org/ at Kainan University on March 17, 2015

*Table 6: Average major element oxide composition of VTR spinels*

| Sample | *n* | $SiO_2$ | $TiO_2$ | $Al_2O_3$ | $Cr_2O_3$ | FeO | MnO | MgO | NiO | Total | Mg-no. | Cr-no. |
|---|---|---|---|---|---|---|---|---|---|---|---|---|
| S1902-05 | 5 | 0·02(3) | 0·06(4) | 41·77(116) | 27·55(87) | 13·45(46) | 0·03(8) | 17·50(44) | 0·20(3) | 100·59(94) | 69·87(114) | 30·68(122) |
| S1902-07 | 4 | 0·02(2) | 0·04(2) | 45·33(215) | 23·05(211) | 13·27(26) | 0·13(4) | 17·32(10) | 0·21(3) | 99·40(47) | 69·95(52) | 25·46(261) |
| S1902-23 | 5 | 0·02(3) | 0·06(4) | 48·56(36) | 20·74(38) | 12·51(30) | 0·14(5) | 18·25(35) | 0·24(5) | 100·52(80) | 72·22(74) | 22·27(23) |
| S1903-03 | 4 | 0·00(0) | 0·07(1) | 43·20(115) | 26·37(85) | 14·09(44) | 0·16(1) | 16·98(26) | 0·18(2) | 100·98(51) | 68·25(99) | 29·06(118) |
| S1903-05 | 8 | 0·01(2) | 0·08(3) | 49·27(88) | 19·19(70) | 13·74(37) | 0·02(2) | 18·36(30) | 0·27(3) | 100·93(56) | 70·43(83) | 20·72(87) |
| S1904-33 | 11 | 0·04(4) | 0·06(3) | 43·79(76) | 24·20(66) | 14·29(35) | 0·13(4) | 16·04(20) | 0·20(4) | 98·77(30) | 66·68(74) | 27·05(86) |
| S1904-38 | 4 | 0·04(3) | 0·08(1) | 44·38(56) | 24·68(50) | 13·03(18) | 0·11(7) | 17·40(29) | 0·24(0) | 99·92(88) | 70·43(59) | 27·17(42) |
| S1904-39 | 4 | 0·02(2) | 0·04(1) | 49·27(133) | 19·37(146) | 13·45(34) | 0·17(0) | 18·10(39) | 0·25(3) | 100·60(92) | 70·58(71) | 20·87(165) |
| S1904-40 | 4 | 0·00(1) | 0·06(2) | 42·39(67) | 26·94(39) | 13·31(24) | 0·15(3) | 17·07(44) | 0·18(3) | 100·13(69) | 69·57(76) | 28·09(59) |
| S1904-42 | 15 | 0·01(2) | 0·06(2) | 44·30(106) | 24·63(92) | 12·92(25) | 0·14(6) | 17·27(36) | 0·24(2) | 99·55(66) | 70·43(62) | 27·17(116) |
| S1905-56 | 4 | 0·01(1) | 0·04(3) | 39·72(186) | 29·76(98) | 13·82(45) | 0·18(1) | 16·48(16) | 0·20(0) | 100·02(115) | 68·01(87) | 33·47(175) |
| S1905-59 | 16 | 0·01(2) | 0·05(3) | 43·84(263) | 23·76(293) | 14·30(72) | 0·13(6) | 16·76(87) | 0·23(5) | 99·19(155) | 67·36(163) | 27·07(176) |
| S1912-04 | 6 | 0·00(0) | 0·09(4) | 48·28(37) | 20·16(70) | 12·70(37) | 0·05(6) | 18·71(20) | 0·31(2) | 100·20(98) | 72·42(70) | 21·88(65) |
| S1912-05 | 6 | 0·03(2) | 0·07(2) | 50·91(19) | 16·27(30) | 13·25(11) | 0·12(3) | 17·83(14) | 0·35(4) | 98·85(43) | 70·59(26) | 17·65(27) |
| S1912-06 | 4 | 0·01(3) | 0·08(3) | 51·16(40) | 17·02(41) | 12·32(28) | 0·07(6) | 18·78(27) | 0·33(1) | 99·62(100) | 73·11(64) | 18·24(28) |
| S1912-08 | 6 | 0·05(4) | 0·08(3) | 49·48(23) | 17·98(30) | 12·91(28) | 0·12(3) | 18·15(24) | 0·31(2) | 99·11(44) | 71·48(67) | 19·60(24) |
| S1912-12 | 4 | 0·00(1) | 0·07(3) | 50·48(26) | 17·71(47) | 12·95(41) | 0·14(3) | 19·09(36) | 0·32(1) | 100·64(42) | 72·44(97) | 19·05(47) |
| S1913-01 | 3 | 0·01(2) | 0·06(1) | 51·02(26) | 17·49(34) | 11·94(9) | 0·07(6) | 18·87(19) | 0·35(3) | 99·81(8) | 73·81(20) | 18·69(36) |
| S1913-07 | 5 | 0·00(0) | 0·08(2) | 52·64(49) | 16·28(37) | 12·90(38) | 0·04(6) | 18·97(21) | 0·30(4) | 101·07(80) | 72·40(61) | 17·18(36) |
| S1913-03 | 4 | 0·03(3) | 0·05(5) | 52·51(87) | 14·70(154) | 13·27(77) | 0·12(3) | 17·90(31) | 0·26(4) | 98·92(69) | 70·63(153) | 15·80(161) |
| S1913-28 | 4 | 0·00(0) | 0·08(3) | 51·20(65) | 17·34(23) | 12·33(15) | 0·14(2) | 19·01(37) | 0·30(1) | 100·36(89) | 73·33(37) | 18·51(37) |
| S1913-36 | 15 | 0·03(2) | 0·07(4) | 49·01(74) | 19·48(93) | 12·13(30) | 0·12(4) | 18·61(21) | 0·29(2) | 99·75(45) | 73·24(54) | 21·05(104) |
| S1920-84 | 4 | 0·00(0) | 0·05(1) | 55·70(44) | 12·43(25) | 11·73(19) | 0·08(4) | 19·60(24) | 0·35(5) | 99·86(62) | 74·86(27) | 13·02(27) |
| S1920-85 | 5 | 0·00(0) | 0·07(2) | 53·91(65) | 13·43(58) | 12·43(18) | 0·11(4) | 19·01(6) | 0·32(3) | 99·27(78) | 73·17(31) | 14·32(62) |
| S1920-88 | 4 | 0·01(2) | 0·09(2) | 53·24(15) | 14·21(49) | 12·15(35) | 0·06(4) | 19·59(26) | 0·33(3) | 99·68(74) | 74·19(79) | 15·18(42) |
| S1923-38 | 7 | 0·00(0) | 0·06(3) | 45·94(101) | 23·54(116) | 12·56(20) | 0·14(2) | 18·07(28) | 0·26(3) | 100·42(43) | 71·94(50) | 25·58(133) |
| S1923-42 | 3 | 0·02(3) | 0·08(3) | 46·74(100) | 23·18(103) | 12·67(24) | 0·00(0) | 18·10(17) | 0·17(2) | 100·85(9) | 71·80(46) | 24·97(123) |
| S1923-45 | 4 | 0·02(2) | 0·06(4) | 44·94(41) | 24·48(10) | 12·35(10) | 0·13(4) | 17·46(34) | 0·20(4) | 99·68(65) | 71·59(56) | 26·76(23) |
| S1923-46 | 9 | 0·03(3) | 0·06(3) | 44·91(48) | 22·78(50) | 13·51(42) | 0·13(3) | 16·77(34) | 0·24(2) | 98·46(92) | 68·88(105) | 25·38(38) |
| S1923-84 | 4 | 0·02(2) | 0·06(3) | 45·80(51) | 23·71(41) | 12·50(22) | 0·12(4) | 18·39(14) | 0·22(3) | 100·79(34) | 72·40(28) | 25·77(46) |
| S1923-86 | 10 | 0·01(2) | 0·05(3) | 45·60(125) | 23·13(148) | 14·06(39) | 0·04(5) | 17·41(31) | 0·21(3) | 100·54(54) | 68·83(87) | 25·39(169) |
| S1924-01 | 2 | 0·02(2) | 0·08(3) | 52·37(85) | 15·90(93) | 12·55(93) | 0·03(4) | 18·84(42) | — | 99·80(66) | 72·80(192) | 16·92(105) |
| S1924-03 | 4 | 0·01(2) | 0·07(3) | 52·40(66) | 16·13(39) | 13·11(30) | 0·07(6) | 18·86(31) | — | 100·70(87) | 71·95(62) | 17·12(49) |
| S1924-04 | 1 | 0·00 | 0·06 | 53·99 | 13·92 | 12·09 | 0·00 | 19·30 | 0·34 | 99·70 | 74·00 | 14·74 |
| S1924-05 | 4 | 0·01(3) | 0·04(2) | 53·00(69) | 15·46(28) | 12·09(19) | 0·07(8) | 19·38(20) | 0·33(4) | 100·39(71) | 74·08(13) | 16·37(41) |
| S1924-12 | 4 | 0·00(0) | 0·07(4) | 52·96(47) | 14·34(18) | 12·70(41) | 0·13(4) | 19·17(13) | 0·33(3) | 99·65(36) | 72·91(67) | 15·37(26) |
| S1924-19 | 5 | 0·04(2) | 0·08(1) | 50·69(25) | 16·45(52) | 12·26(18) | 0·14(3) | 18·15(24) | 0·32(3) | 98·15(52) | 72·52(35) | 17·87(51) |
| S1925-05 | 7 | 0·02(3) | 0·07(4) | 52·66(79) | 15·41(50) | 12·57(32) | 0·04(2) | 19·47(18) | 0·31(3) | 100·56(85) | 73·41(44) | 16·41(61) |
| S1925-71 | 5 | 0·03(2) | 0·05(2) | 47·08(25) | 22·04(16) | 13·50(26) | 0·15(5) | 17·79(15) | 0·23(1) | 100·88(48) | 70·14(46) | 23·89(11) |
| S1925-77 | 6 | 0·02(2) | 0·09(2) | 44·58(31) | 24·18(51) | 12·49(43) | 0·14(3) | 17·62(23) | – | 100·29(70) | 72·40(123) | 26·78(35) |
| S1927-01 | 4 | 0·00(0) | 0·05(1) | 45·44(25) | 23·17(33) | 13·25(31) | 0·10(1) | 18·20(29) | 0·22(3) | 100·39(73) | 71·01(64) | 25·48(24) |
| S1927-02 | 6 | 0·05(2) | 0·04(2) | 46·43(95) | 22·00(88) | 13·19(30) | 0·12(2) | 17·03(20) | 0·22(3) | 99·07(38) | 69·72(72) | 24·12(107) |
| S1927-03 | 4 | 0·00(0) | 0·07(1) | 45·80(62) | 22·79(26) | 13·00(27) | 0·14(1) | 17·83(12) | 0·22(3) | 99·87(77) | 70·98(52) | 25·02(27) |
| S1927-05 | 4 | 0·01(1) | 0·04(3) | 47·45(52) | 22·60(21) | 12·95(35) | 0·14(3) | 17·94(23) | 0·26(2) | 101·30(59) | 71·17(75) | 24·21(30) |
| S1928-09 | 5 | 0·03(4) | 0·09(2) | 46·94(61) | 21·69(23) | 13·00(21) | 0·13(2) | 18·16(28) | 0·28(4) | 100·28(89) | 71·34(48) | 23·66(28) |
| S1928-10 | 4 | 0·03(3) | 0·05(2) | 46·42(18) | 21·89(59) | 13·06(28) | 0·13(2) | 17·92(23) | 0·24(1) | 99·67(93) | 70·98(56) | 24·03(51) |
| S1928-13 | 3 | 0·03(1) | 0·05(2) | 46·73(38) | 21·70(93) | 13·31(25) | 0·00(0) | 17·82(13) | 0·17(3) | 99·86(71) | 70·49(53) | 23·75(92) |
| S1928-14 | 8 | 0·03(2) | 0·07(2) | 47·49(80) | 20·04(58) | 12·81(36) | 0·01(3) | 18·26(26) | 0·26(3) | 98·96(112) | 71·76(61) | 22·06(69) |

Downloaded from http://petrology.oxfordjournals.org/ at Kainan University on March 17, 2015

| Sample | *n* | $SiO_2$ | $TiO_2$ | $Al_2O_3$ | $Cr_2O_3$ | FeO | MnO | MgO | NiO | Total | Mg-no. | Cr-no. |
|---|---|---|---|---|---|---|---|---|---|---|---|---|
| S1928-15 | 5 | 0·02(3) | 0·07(4) | 46·61(99) | 21·86(123) | 13·79(30) | 0·03(3) | 17·83(27) | 0·25(2) | 100·40(71) | 69·75(55) | 23·93(138) |
| S1928-19 | 4 | 0·03(3) | 0·09(3) | 46·76(37) | 21·35(53) | 12·94(21) | 0·13(1) | 18·09(32) | 0·27(3) | 99·64(39) | 71·36(43) | 23·45(57) |
| S1930-15 | 5 | 0·03(4) | 0·05(3) | 36·15(85) | 31·74(99) | 16·07(52) | 0·15(1) | 16·10(36) | 0·19(4) | 100·41(52) | 64·11(112) | 37·07(127) |
| S1930-70 | 5 | 0·03(2) | 0·07(2) | 35·51(87) | 31·60(98) | 15·61(38) | 0·03(5) | 16·73(28) | — | 99·62(83) | 65·64(53) | 37·38(126) |
| S1930-79 | 3 | 0·02(2) | 0·06(2) | 35·01(78) | 32·78(89) | 15·87(17) | 0·00(0) | 15·68(35) | 0·24(1) | 99·62(70) | 63·78(27) | 35·58(117) |
| S1930-134 | 5 | 0·00(0) | 0·07(3) | 37·33(88) | 29·90(105) | 17·17(24) | 0·17(7) | 15·54(12) | 0·18(3) | 100·36(58) | 61·75(26) | 34·95(128) |
| S2209-01 | 5 | 0·02(1) | 0·05(1) | 39·16(50) | 28·13(42) | 15·13(34) | 0·00(0) | 16·29(13) | 0·07(5) | 99·05(63) | 65·75(39) | 32·51(47) |
| S2218-01 | 3 | 0·02(2) | 0·06(1) | 44·80(64) | 21·26(23) | 17·62(63) | 0·00(0) | 15·13(45) | 0·20(4) | 99·15(38) | 60·49(154) | 24·15(45) |
| S2220-04 | 7 | 0·01(2) | 0·06(3) | 43·58(87) | 25·02(52) | 13·83(80) | 0·14(3) | 17·30(57) | 0·22(4) | 100·05(73) | 69·04(193) | 27·80(71) |
| S2220-06 | 4 | 0·04(3) | 0·07(4) | 44·13(194) | 23·64(164) | 16·08(77) | 0·17(4) | 16·57(50) | 0·20(1) | 100·99(16) | 64·75(177) | 26·46(220) |
| S2221-01 | 4 | 0·02(1) | 0·06(3) | 47·12(108) | 21·45(149) | 12·41(33) | 0·00(0) | 18·00(39) | 0·22(4) | 99·31(48) | 72·11(96) | 23·39(165) |
| S2221-04 | 2 | 0·01(2) | 0·07(2) | 45·02(134) | 23·54(170) | 13·46(33) | 0·15(2) | 17·68(30) | 0·25(5) | 100·02(37) | 70·08(67) | 25·97(136) |
| S2221-05 | 5 | 0·00(0) | 0·07(2) | 44·98(56) | 23·75(19) | 12·91(26) | 0·12(2) | 17·67(19) | 0·20(1) | 99·59(72) | 70·94(23) | 26·15(27) |
| VE1-1 | 6 | 0·01(2) | 0·05(1) | 51·60(36) | 17·59(79) | 12·32(25) | 0·13(3) | 18·85(26) | 0·31(3) | 100·80(103) | 73·13(56) | 18·61(75) |
| VE1-2 | 2 |  | 0·05(2) | 48·79(250) | 19·71(299) | 13·90(53) | 0·01(1) | 18·33(25) | 0·26(2) | 101·29(19) | 70·19(40) | 21·34(338) |
| VE1-3 | 4 | 0·01(1) | 0·06(2) | 49·65(47) | 17·95(35) | 13·16(10) | 0·13(3) | 18·09(19) | 0·24(3) | 99·00(14) | 70·93(29) | 19·52(34) |
| VE1-5 | 5 | 0·02(2) | 0·07(2) | 46·81(47) | 21·59(41) | 13·61(28) | 0·14(2) | 18·03(20) | 0·26(2) | 100·10(41) | 70·21(40) | 23·62(32) |
| VE1-7 | 4 | 0·00(0) | 0·05(3) | 48·79(67) | 19·82(61) | 12·87(19) | 0·13(2) | 18·15(25) | 0·25(2) | 99·92(109) | 71·47(45) | 21·43(63) |
| VE 4-4 | 3 | 0·00(0) | 0·06(4) | 43·17(177) | 25·92(173) | 13·67(8) | 0·02(2) | 17·83(5) | 0·17(4) | 100·73(35) | 69·91(6) | 28·74(216) |
| VE 4-7 | 4 | 0·04(3) | 0·05(2) | 46·47(56) | 22·68(80) | 12·96(26) | 0·14(1) | 18·01(19) | 0·21(2) | 100·26(40) | 71·15(38) | 24·66(86) |
| P7003-19-J | 3 | 0·02(1) | 0·10(1) | 41·12(78) | 30·19(57) | 12·96(27) | 0·12(5) | 17·21(34) | 0·15(3) | 100·54(87) | 70·34(27) | 33·01(6) |
| P7003-23-A | 5 | 0·00(0) | 0·06(2) | 38·99(93) | 30·00(105) | 14·66(62) | 0·05(3) | 16·27(32) | — | 99·95(88) | 66·43(139) | 34·04(128) |
| CH78 DR10-1 | 4 | 0·02(2) | 0·08(4) | 46·67(3·17) | 22·10(3·21) | 14·12(50) | — | 17·82(64) | 0·19(3) | 101·03(43) | 69·21(151) | 24·16(388) |
| EW12-5 | 5 | 0·01(1) | 0·05(2) | 48·97(86) | 19·46(59) | 11·89(24) | 0·00(0) | 18·70(25) | 0·33(7) | 99·40(42) | 73·71(56) | 21·05(76) |
| EW13-7 | 4 | 0·01(1) | 0·08(2) | 45·88(49) | 22·51(48) | 12·89(35) | 0·00(0) | 18·09(29) | 0·23(1) | 99·70(67) | 71·45(77) | 24·76(55) |
| EW16-1 | 3 | 0·03(4) | 0·07(3) | 46·96(160) | 21·40(190) | 13·06(45) | 0·00(0) | 17·52(18) | 0·23(2) | 99·27(52) | 70·52(64) | 23·41(220) |
| EW16-5 | 5 | 0·00(1) | 0·07(2) | 46·18(43) | 22·62(42) | 13·83(18) | 0·18(9) | 17·85(30) | 0·23(3) | 101·15(52) | 70·08(45) | 24·70(54) |
| EW16-6 | 5 | 0·03(4) | 0·07(3) | 43·79(128) | 24·02(85) | 14·02(17) | 0·00(0) | 17·10(32) | 0·24(3) | 99·28(70) | 68·49(54) | 26·91(126) |
| EW16-7 | 8 | 0·02(2) | 0·07(2) | 44·24(63) | 23·94(57) | 13·96(17) | 0·14(3) | 17·32(30) | 0·22(2) | 99·81(65) | 68·86(52) | 26·63(70) |
| EW17-3 | 9 | 0·00(1) | 0·08(2) | 46·27(64) | 21·92(39) | 12·84(37) | 0·01(1) | 17·86(33) | 0·26(6) | 99·25(97) | 71·26(54) | 24·12(48) |
| RC21-13AC | 4 | 0·06(4) | 0·06(3) | 37·64(22) | 30·48(81) | 15·08(17) | 0·15(2) | 16·81(28) | 0·19(3) | 100·42(66) | 66·52(36) | 35·19(49) |

*n*, number of analyses; 1σ standard deviation in parentheses refers to the last digit.

with orthopyroxene and spinel and positive $TiO_2$ vs $Na_2O$ (Fig. 2) are consistent with partial melting trends (Michael & Bonatti, 1985). The Mg-number of the residual clinopyroxene varies between 89·4 and 93·4, showing a weak correlation with major and minor elements. In general, the most incompatible element-depleted samples have higher clinopyroxene Mg-number, consistent with a partial melting trend. However, the observed sample-scale variation overlaps the entire VTR range.

Clinopyroxene REE patterns along the VLS are, on the whole, strongly depleted in light REE (LREE) relative to middle (MREE) and heavy REE (HREE), similar to residual peridotites collected elsewhere along mid-ocean ridges (Johnson *et al.*, 1990; Johnson & Dick, 1992; Ross & Elthon, 1997; Hellebrand *et al.*, 2001, 2002, 2003, N-type; Brunelli *et al.*, 2003; Fig. 3a). $Yb_{(N)}$ is 3–10 times chondritic (Anders & Grevesse, 1989). $Dy/Yb_{(N)}$ varies between 0·54 (S1930-79) and 1·14 (S1913-36). $Sm/Yb_{(N)}$ varies between 0·05 (AT83) and 0·58 (S1925-56). $Ce/Yb_{(N)}$ ranges from 0·00025 (S1927-02) to 0·029 (S1924-01). Both $Dy/Yb_{(N)}$ and $Sm/Yb_{(N)}$ show an overall (weak) positive correlation with $Yb_{(N)}$ (i.e. REE patterns with lower $Yb_{(N)}$ have steeper slopes, Fig. 3b). With respect to these trends, the dispersion increases from HREE to MREE and LREE as revealed by the non-parallel REE patterns in Fig. 3a. LREE abundances, here represented by the $Ce/Yb_{(N)}$ ratio, do not show any obvious correlation with $Yb_{(N)}$ (Fig. 3b).

Ti and Zr concentrations range from 328 to 1624 ppm and from 0·07 to 2·77 ppm, respectively, spanning the abyssal peridotite field. Significantly, few samples plot in the most depleted part of the global data array (Fig. 3c). The distribution of these elements is marked by a wide dispersion, as observed for the LREE. Zr contents, close



Downloaded from http://petrology.oxfordjournals.org/ at Kainan University on March 17, 2015

*Table 7: Average trace element (ppm) composition of VTR clinopyroxenes*

| Sample | *n* | Sc | Ti | V | Cr | Sr | Y | Zr | Cs | Ba | La | Ce | Nd | Sm | Eu | Gd | Dy | Er | Yb |
|---|---|---|---|---|---|---|---|---|---|---|---|---|---|---|---|---|---|---|---|
| S1902-05 | 1 | 56 | 649 | 224 | 9213 | 0·80 | 6·34 | 0·46 | 0·00 | 0·20 | 0·00 | 0·04 | 0·19 | 0·20 | 0·13 | 0·54 | 0·98 | 0·61 | 0·71 |
| S1903-05 | 2 | 56(1) | 1109(52) | 255(7) | 8335(161) | 0·41(6) | 11·07(71) | 0·58(1) | 0·00 | 0·00 | 0·08(11) | 0·01(0) | 0·26(4) | 0·41(6) | 0·14(3) | 0·77(6) | 1·17(13) | 0·98(18) | 1·20(23) |
| S1904-33 | 2 | 49(4) | 944(11) | 251(6) | 8960(130) | 0·37(5) | 6·83(33) | 0·29(2) | — | 0·01(2) | 0·00(0) | 0·01(0) | 0·06(1) | 0·12(2) | 0·09(9) | 0·46(1) | 0·93(2) | 0·73(3) | 0·82(11) |
| S1904-42 | 5 | 46(3) | 625(116) | 213(7) | 8887(569) | 0·79(34) | 6·30(63) | 0·38(9) | 0·13(4) | 0·20(18) | 0·01(2) | 0·03(2) | 0·21(9) | 0·24(8) | 0·12(3) | 0·50(9) | 0·93(9) | 0·71(10) | 0·78(10) |
| S1912-05 | 1 | 46 | 869 | 230 | 7040 | 0·30 | 8·87 | 0·30 | — | 0·03 | 0·00 | 0·01 | 0·15 | 0·25 | 0·12 | 0·63 | 1·35 | 0·89 | 0·90 |
| S1912-08 | 1 | 52 | 1070 | 230 | 8077 | 0·50 | 11·39 | 1·00 | — | 0·10 | 0·01 | 0·02 | 0·27 | 0·42 | 0·20 | 0·88 | 1·58 | 1·32 | 1·20 |
| S1913-03 | 1 | 54 | 1444 | 245 | 8843 | 2·60 | 14·2 | 1·80 |  | 1·67 | 0·03 | 0·04 | 0·64 | 0·67 | 0·33 | 1·38 | 2·43 | 1·48 | 1·46 |
| S1913-36 | 2 | 51(0) | 1497(209) | 230(1) | 9379(521) | 1·82(30) | 12·97(38) | 2·77(52) | — | 0·14(11) | 0·01(0) | 0·10(4) | 0·75(4) | 0·65(9) | 0·35(4) | 1·27(10) | 2·14(14) | 1·30(7) | 1·26(2) |
| S1920-84 | 1 | 54 | 1411 | 246 | 7000 | 1·10 | 14·47 | 1·63 | 0·27 | 0·00 | 0·00 | 0·06 | 0·35 | 0·61 | 0·30 | 1·30 | 1·97 | 1·71 | 1·40 |
| S1923-42 | 1 | 53 | 832 | 230 | 8888 | 0·50 | 9·07 | 0·26 | 0·00 | 0·30 | 0·01 | 0·03 | 0·18 | 0·28 | 0·18 | 0·79 | 1·40 | 1·08 | 1·03 |
| S1923-45 | 2 | 50·3(1) | 681(68) | 241(2) | 8887(224) | 0·25(7) | 6·99(9) | 0·10(0) | — | 0·15(21) | 0·00(0) | 0·01(0) | 0·05(1) | 0·09(1) | 0·07(1) | 0·41(4) | 0·99(12) | 0·79(9) | 0·77(3) |
| S1923-46 | 1 | 59 | 819 | 267 | 8978 | 0·40 | 8·66 | 0·20 | — | 0·06 | 0·00 | 0·02 | 0·11 | 0·18 | 0·13 | 0·64 | 1·23 | 0·80 | 0·93 |
| S1924-01 | 2 | 59·8(1) | 1164(31) | 264(4) | 8333(104) | 1·7(8) | 12·41(1) | 2·7(17) | — | 1·2(11) | 0·06(7) | 0·15(11) | 0·58(10) | 0·57(8) | 0·27(1) | 1·08(12) | 1·74(17) | 1·31(7) | 1·4(13) |
| S1924-03 | 2 | 46(1) | 1098(54) | 230(5) | 7352(29) | 0·49(11) | 10(54) | 0·70(4) | 0·03(4) | 0·06(5) | 0·00 | 0·02(0) | 0·28(2) | 0·39(7) | 0·20(2) | 0·95(6) | 1·51(12) | 1·25(7) | 1·11(9) |
| S1924-04 | 1 | 49 | 1089 | 218 | 6413 | 0·79 | 10·97 | 0·93 | 0·00 | 0·33 | 0·00 | 0·02 | 0·30 | 0·41 | 0·24 | 1·17 | 1·96 | 1·25 | 1·26 |
| S1924-19 | 2 | 48·4(3) | 1189(10) | 226(1) | 7739(105) | 0·70(0) | 12·34(34) | 1·10(0) | — | 0·08(4) | 0·00(0) | 0·03(0) | 0·40(6) | 0·49(4) | 0·23(2) | 1·02(8) | 1·84(6) | 1·31(16) | 1·35(11) |
| S1925-56 | 1 | 48 | 1624 | 325 | 9337 | 0·57 | 8·08 | 0·50 | 0·00 | 0·08 | 0·01 | 0·02 | 0·24 | 0·42 | 0·16 | 0·91 | 1·27 | 0·73 | 0·80 |
| S1925-71 | 2 | 52(5) | 812(122) | 244(13) | 8594(426) | 0·85(7) | 8·29(73) | 0·50(0) | — | 0·05(7) | 0·01(0) | 0·05(1) | 0·15(2) | 0·19(2) | 0·12(0) | 0·66(6) | 1·21(2) | 0·87(1) | 1·02(4) |
| S1925-77 | 4 | 34(1) | 560(32) | 187(4) | 8572(241) | 0·60(9) | 5·52(32) | 0·47(5) | — | 0·04(5) | 0·01(1) | 0·03(1) | 0·21(0) | 0·21(2) | 0·12(1) | 0·52(8) | 0·90(13) | 0·58(9) | 0·59(4) |
| S1927-01 | 1 | 56 | 941 | 288 | 8909 | 0·38 | 8·56 | 0·27 | — | 0·10 | 0·01 | 0·02 | 0·11 | 0·20 | 0·11 | 0·57 | 1·25 | 1·13 | 1·00 |
| S1927-02 | 1 | 63 | 884 | 296 | 9167 | 0·38 | 8·52 | 0·27 | — | 0·13 | 0·01 | 0·00 | 0·09 | 0·22 | 0·11 | 0·51 | 1·22 | 0·94 | 1·07 |
| S1927-05 | 2 | 59(2) | 649(9) | 254(1) | 8620(78) | 0·48(12) | 7·83(49) | 0·30(5) | 0·00 | 0·00 | 0·02(1) | 0·03(1) | 0·15(7) | 0·18(3) | 0·08(3) | 0·42(1) | 1·25(8) | 1·00(3) | 1·03(6) |
| S1928-09 | 1 | 50 | 799 | 216 | 8349 | 0·31 | 8·88 | 0·36 | 0·00 | 0·19 | 0·02 | 0·02 | 0·25 | 0·35 | 0·20 | 0·78 | 1·18 | 0·71 | 0·73 |
| S1930-79 | 2 | 51(1) | 415(26) | 252(31) | 10290(945) | 2·00(137) | 4·25(37) | 2·26(174) | 0·00(0) | 0·49(46) | 0·15(16) | 0·04(1) | 0·10(6) | 0·08(3) | 0·05(1) | 0·23(6) | 0·55(4) | 0·53(1) | 0·53(7) |
| S2209-01 | 2 | 49(3) | 472(20) | 226(3) | 9366(6) | 0·57(42) | 4·55(59) | 0·16(2) | 0·00 | 0·02(3) | 0·00 | 0·00 | 0·05(0) | 0·08(0) | 0·05(1) | 0·25(3) | 0·66(11) | 0·54(9) | 0·60(6) |
| S2220-06 | 2 | 54(3) | 644(33) | 235(18) | 9857(826) | — | 6·56(55) | 0·17(1) | 0·02(3) | 0·30(39) | 0·07(9) | 0·02(2) | 0·10(8) | 0·15(2) | 0·10(1) | 0·47(8) | 0·99(10) | 0·80(4) | 0·80(9) |
| S2221-04 | 3 | 55(1) | 788(66) | 254(9) | 9805(430) | 2·34(29) | 7·93(49) | 0·48(11) | 0·13(3) | 0·60(30) | 0·03(1) | 0·07(2) | 0·19(1) | 0·23(1) | 0·12(2) | 0·56(4) | 1·25(7) | 0·90(9) | 0·99(5) |
| S2221-05 | 2 | 54(1) | 1040(6) | 262(1) | 9724(103) | 0·40(0) | 8·52(8) | 0·25(7) | — | 0·06(1) | 0·00(0) | 0·00(0) | 0·07(1) | 0·16(2) | 0·12(1) | 0·57(5) | 1·15(11) | 0·96(4) | 1·01(3) |
| VE1-1 | 2 | 55(1) | 1080(13) | 265(14) | 8975(47) | 0·50(0) | 11·42(48) | 0·58(4) | — | 0·00(0) | 0·00(0) | 0·02(1) | 0·28(8) | 0·33(3) | 0·22(1) | 0·92(4) | 1·61(3) | 1·34(9) | 1·20(1) |
| VE1-5 | 3 | — | 888(76) | 291(6) | — | 1·50(71) | — | 0·55(7) | — | — | — | 0·01(1) | 0·13(3) | 0·23(7) | 0·14(2) | — | 1·09(12) | 0·75(10) | 0·82(10) |
| VE 4-7 | 2 | — | 781(75) | 269(24) | 7876 | 1·80(28) | 6·70 | 0·50(14) | — | — | — | 0·01(1) | 0·11(1) | 0·20(1) | 0·13(2) | — | 1·22(25) | 0·81(10) | 0·96(11) |
| AT83A | 1 | 45 | 351 | 225 | 9768 | 0·30 | 2·79 | 0·07 | 0·00 | 0·06 | 0·01 | 0·01 | 0·01 | 0·02 | 0·02 | 0·10 | 0·36 | 0·35 | 0·42 |
| EW13-7 | 1 | 59 | 958 | 212 | 8013 | 0·46 | 9·45 | 0·38 | 0·00 | 0·02 | 0·00 | 0·01 | 0·25 | 0·31 | 0·14 | 0·80 | 1·46 | 1·03 | 1·02 |
| EW16-1 | 2 | 51(2) | 890(13) | 247(3) | 8980(4) | 0·72(59) | 7·04(23) | 0·44(6) | — | 0·23(15) | 0·01(1) | 0·01(1) | 0·12(2) | 0·22(2) | 0·13(1) | 0·60(7) | 1·13(1) | 0·76(7) | 0·79(6) |
| EW16-5 | 1 | 54 | 829·00 | 219·00 | 8220·00 | 0·49 | 7·66 | 0·68 | 0·00 | 0·09 | 0·00 | 0·01 | 0·16 | 0·26 | 0·10 | 0·58 | 1·42 | 1·11 | 1·14 |

*n*, number of analyses; 1σ standard deviation in parentheses refers to the last digit.





Downloaded from http://petrology.oxfordjournals.org/ at Kainan University on March 17, 2015

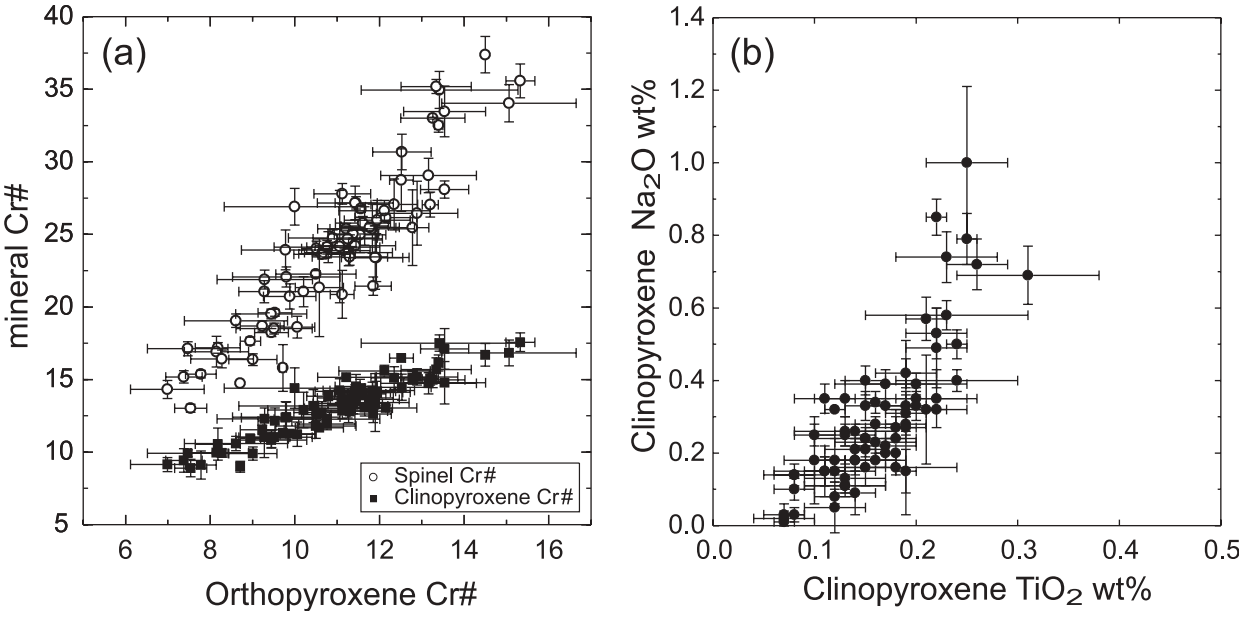


**Fig. 2.** Residual mineral composition sample averages. (a) Orthopyroxene vs spinel and clinopyroxene Cr-number [100 × Cr/(Cr + Al)]. Bars represent 1σ sample variations. (b) $TiO_2$ vs $Na_2O$ content (wt %) of residual clinopyroxene from the Vema Lithospheric Section.

to the detection limits, are responsible for part of the measured scatter.

### Major element variability along the VLS

Figure 4 shows the mineral major element compositional variation vs longitude. Given that the VLS is oriented along a sea-floor spreading flow line, the distance from the ridge axis gives a good approximation of relative crustal ages. The westernmost (sector C) peridotites are the more Al–Ti-rich/Cr-poor rocks of the entire sequence; they are the oldest sampled along the VLS, ranging between 18·5 and 19·6 Ma [ages have been estimated using spreading rates after Cande *et al.* (1988)]. The easternmost samples (from 1·5 to 7·5 Ma) are, on average, more depleted in incompatible elements than samples from the other sectors. The overall trend along the 20 Myr lithospheric section shows an increase in the degree of depletion of the rocks moving eastward, i.e. towards younger crustal ages.

A well-sampled central region, from 42°23′ to 43°05′W, is characterized by a weak opposite trend with respect to the entire VLS. On average, there is a weak increase in the relative abundance in incompatible elements moving eastward, as shown by an increase in the pyroxene Al and Ti contents, and a decrease in spinel Cr-number (Fig. 4).

Even though there is strong inter- and intra-site variability along the lithospheric section, the overall synchronous variation of mineral chemistry indicates equilibration of the samples in the spinel stability field.

## DISCUSSION

The overall mineral chemistry (high Mg-number and Cr-number, low Ti and Na in clinopyroxene, low modal clinopyroxene and strong depletion in incompatible trace elements) suggests that the VLS peridotites are residues after extraction of a basaltic component. The strong depletion of LREE relative to MREE and HREE suggests a near fractional melting process (Fig. 3a). The peridotites were finally equilibrated under the *P–T* conditions of the spinel peridotite field as shown by the mineral assemblage and chemistry (normative plagioclase is still present in the less-depleted peridotites, but crystallizes only in mylonitic samples; Cannat & Seyler, 1995). The good correlation shown by spinel, orthopyroxene and clinopyroxene Al–Cr distribution indicates equilibrium between these phases and the near absence of re-equilibration in the plagioclase stability field during upwelling (Figs 2 and 4).

### Time-dependent mantle compositional variations along the VLS

Bonatti *et al.* (2003) recognized synchronous variations in the mineral chemistry of the mantle-derived ultramafics and in the thickness of the associated basaltic crust estimated by inversion of gravity and seismic data. A straightforward interpretation is that the observed compositional variations (Fig. 4) result from extraction of variable amounts of mid-ocean ridge basalt (MORB) melt components from a compositionally homogeneous mantle source. Each sample site represents a snapshot of



Downloaded from http://petrology.oxfordjournals.org/ at Kainan University on March 17, 2015

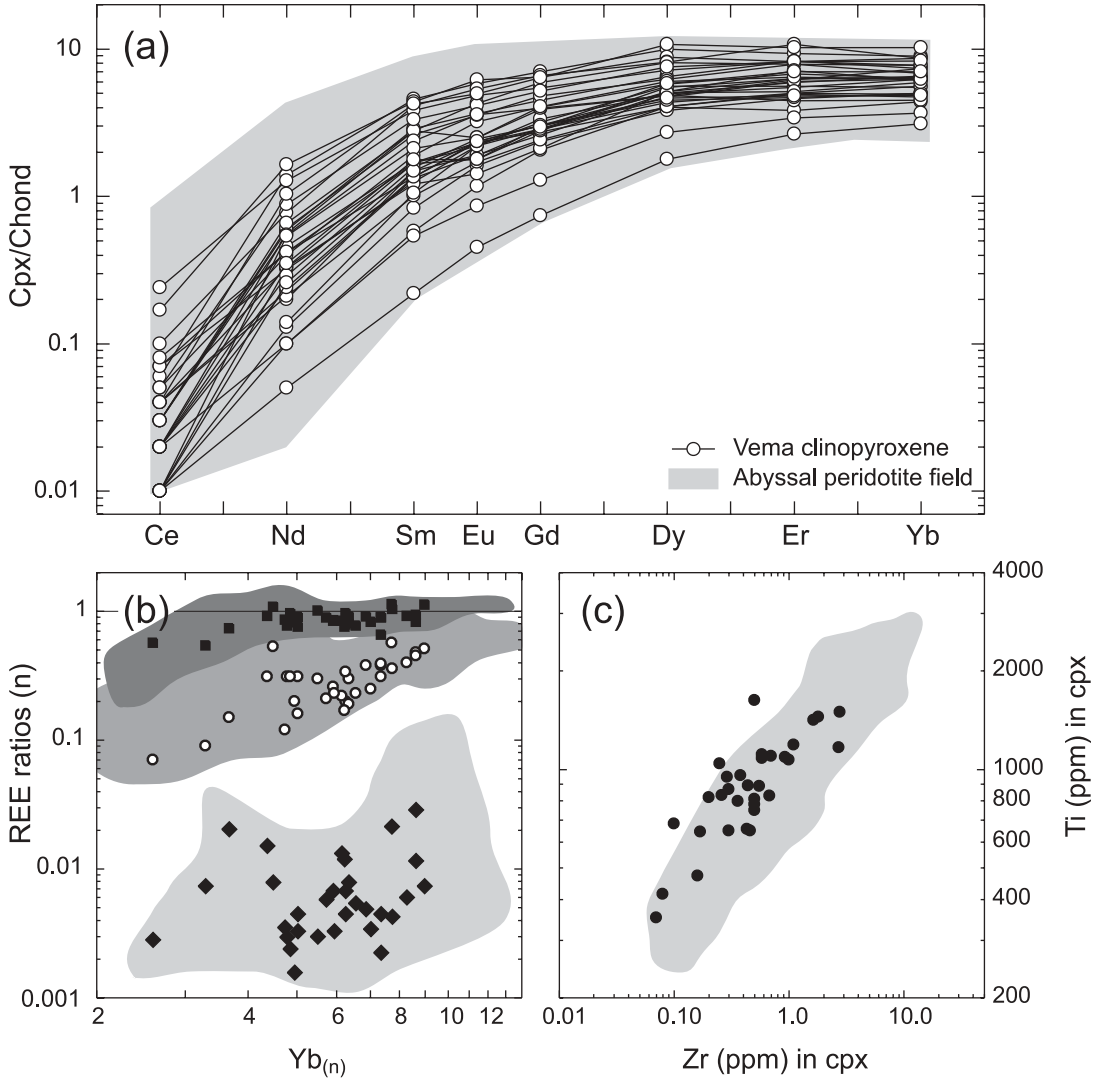


**Fig. 3.** Trace element distribution in residual clinopyroxenes from the Vema Lithospheric Section. (a) Chondrite-normalized clinopyroxene REE patterns for selected samples, normalized to the chondritic values of Anders & Grevesse (1989); the abyssal peridotite field is plotted for comparison. (b) Variation of $Dy/Yb_{(n)}$ (■; dark grey: abyssal peridotite field), $Sm/Yb_{(n)}$ (○; medium grey: abyssal peridotite field) and $Ce/Yb_{(n)}$ (♦; light grey: abyssal peridotite field) vs $Yb_{(n)}$ in the clinopyroxene of the Vema Lithospheric Section peridotites; abyssal peridotite field is plotted for comparison. (c) Clinopyroxene Ti vs Zr contents (ppm) in the Vema Lithospheric Section samples and the abyssal peridotite field (grey).

the continuous melting process that generates the oceanic lithosphere at the ridge axis. Thus, the evolution of the mineral chemistry can be read as evolution in time of the degree of melting undergone by the mantle upwelling below the ridge axis. Figure 4 shows that mantle depletion was stronger in the younger (easternmost) portion of the VLS (e.g. lower Al contents of clinopyroxenes), and weaker in the older (westernmost) one. The resulting overall trend suggests an increase of the degree of melting with time in the last 20 Myr (Bonatti *et al.*, 2003). A 'middle age' period, from 11·9 to 16·4 Ma, in which a weak opposite trend of decreasing degree of melting with time can be recognized, includes residual peridotites from sectors A and B. This observation is in agreement with the inferred secondary nature of the amphibole-bearing ultramafics recovered preferentially in sector B (Cipriani *et al.*, in preparation). During this phase the average degree of melting undergone by the mantle decreased slightly, even though continuous variation is still shown. These short wavelength oscillations have been ascribed to short, buoyancy-driven, thermal pulses in the low-viscosity layer at the base of the melting column (Bonatti *et al.*, 2003). The easternmost samples (site S2209) reveal that the degree of melting undergone by the mantle increased to a relative maximum, leaving the least fertile residues in the youngest part of the VLS.



Downloaded from http://petrology.oxfordjournals.org/ at Kainan University on March 17, 2015

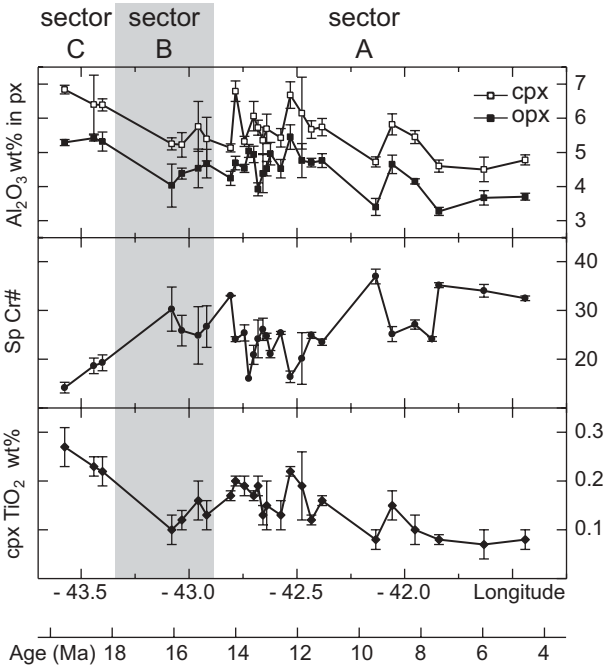


**Fig. 4.** Major element mineral compositions (core average per site $\pm 1\sigma$) in peridotites sampled along the base of the Vema Lithospheric Section. The ridge axis is located at 40°53′W. Each site represents a portion of mantle emplaced at the ridge axis during a time interval that becomes older moving westward. The time scale shows the age (Ma) of the associated magmatic crust based on spreading rates after Cande *et al.* (1988). Samples are grouped in three sectors according to their petrography; the sectors have no age significance (see text).

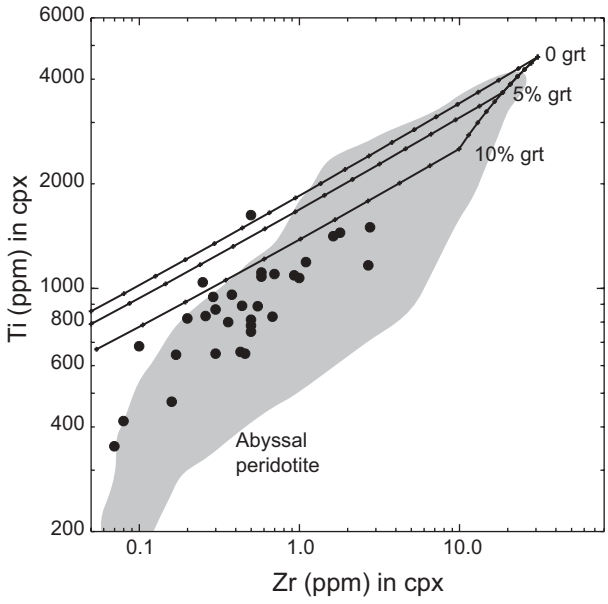


**Fig. 5.** Ti vs Zr (ppm) in the clinopyroxenes of the Vema Lithospheric Section compared with non-modal fractional paths after 0% (spinel field), 5% and 10% partial melting in the garnet field followed by melting in the spinel field. The clinopyroxene compositions are recalculated to those of low-*P* (spinel field) equilibrated clinopyroxene. Abyssal peridotite field is plotted for comparison (grey shading).

## Trace elements in the residual assemblage: a check for fractional melting

Trace element compositions of residual clinopyroxene [high field strength elements (HFSE) and REE] have been used to evaluate the degree of melting undergone by a mantle source in samples with the same characteristics as the VLS peridotites (Johnson *et al.*, 1990; Johnson & Dick, 1992; Hellebrand *et al.*, 2001). Ti and Zr contents in clinopyroxene can be used to model both mechanisms and degree of partial melting of the source (Johnson *et al.*, 1990). Non-modal fractional melting fails to describe the observed trend and dispersion (Fig. 5; see the Appendix for model parameters and functions). Melting in the spinel field cannot reproduce the observed slope and dispersion. Garnet stability field melting does not help to reproduce either the field or the slope defined by the VLS samples, unless we assume unrealistically high degrees (>10%) of melting.

REE ratios in residual clinopyroxene are compared with expected non-modal fractional melting paths in Fig. 6. A major problem concerning model mineral composition curves for partial melting in the garnet stability field arises from the observation that all the studied samples have equilibrated in the spinel field, preventing a direct comparison. During garnet breakdown chemical constituents are redistributed among the spinel field mineral phases. Consequently, we have 'equilibrated' or 'projected' (according to Hellebrand *et al.*, 2002) the garnet part of the model curves into the spinel field by distributing modelled trace elements among the equivalent spinel field mineral assemblage (see Appendix). The resulting clinopyroxene compositional paths plotted in Fig. 6 are, therefore, those of clinopyroxene equilibrated in the spinel facies even for the garnet part of the curve and not those of a clinopyroxene in equilibrium with garnet. $Ce/Yb_{(N)}$, $Sm/Yb_{(N)}$ and $Dy/Yb_{(N)}$ ratios, plotted against $Yb_{(N)}$, describe the depletion of a more incompatible versus a less incompatible element and at the same time provide information on the shape of the REE pattern. Assuming that the REE patterns are generated by a single melting event, we expect that the different ratios will match, simultaneously, a given melting path. Figure 6 shows that melting in the spinel field cannot account for the overall REE distribution. Modeled MREE and HREE contents are too enriched relative to those of the Vema clinopyroxenes. Partial melting in the garnet field appears to match the REE patterns much better. We calculated melting paths after 5 and 10% melting in the garnet field followed by instantaneous garnet–spinel transition and subsequent melting in the spinel field (see Appendix). This leads to MREE ($Sm/Yb_{(N)}$) and HREE ($Dy/Yb_{(N)}$) depletion close to



Downloaded from http://petrology.oxfordjournals.org/ at Kainan University on March 17, 2015

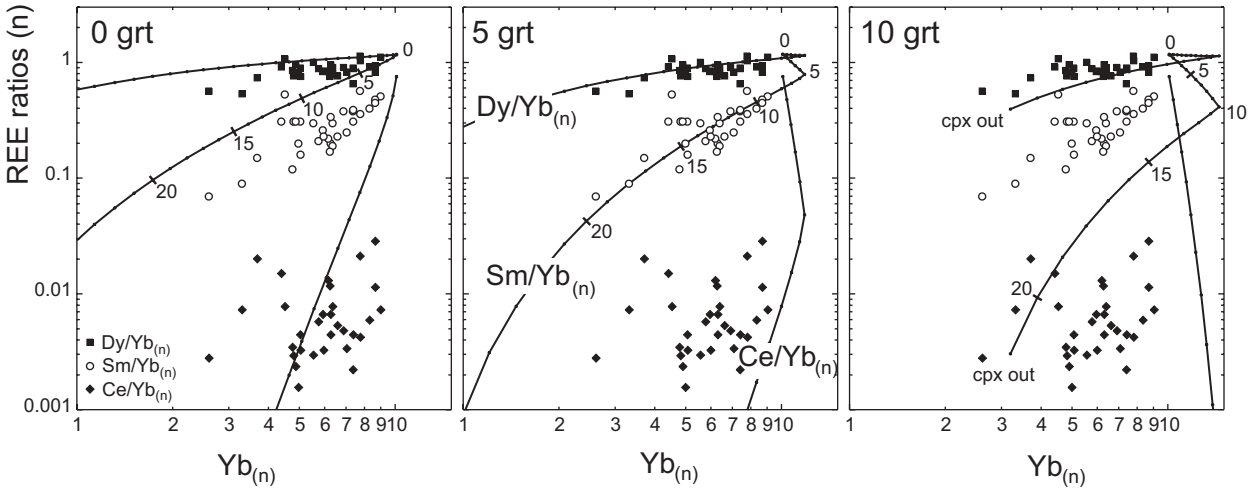


**Fig. 6.** Variation of $Dy/Yb_{(n)}$, $Sm/Yb_{(n)}$ and $Ce/Yb_{(n)}$ vs $Yb_{(n)}$ showing model fractional (non-modal) melting paths varying the degree of melting in the garnet field from 0 to 10% compared with the Vema Lithospheric Section clinopyroxenes. All curves are calculated for a low-*P* (spinel field) equilibrated clinopyroxene. Tick marks on the model curve are 1% melting steps. The total extent of melting (5% increments) is reported for reference on the $Sm/Yb_{(n)}$ melting curve.

that measured in the Vema residual clinopyroxenes, suggesting that the Vema peridotites experienced ≤10% melting in the garnet field. However, REE ratios are not simultaneously matched. The 'mismatch' appears to increase systematically from the HREE to the LREE, suggesting a problem with the chosen model.

## Dynamic vs fractional melting: effect of critical mass porosity

Fractional (non-modal) melting, used in the previous section, assumes that melt is generated and instantaneously completely extracted from the source. Theory and experiments, such as the MELT experiment beneath the East Pacific Rise (Forsyth *et al.*, 1998), suggest that a finite porosity (1–2%) is present during mantle partial melting. The porosity threshold to allow melt migration is estimated at 0·1% at the onset of melting, where low-viscosity volatile-rich melts are expected (Faul, 2001). It is not clear how efficiently this melt is extracted from the source, or, in other words, how much melt remains trapped at the end of the melting process. An approximation of such a process is represented by dynamic melting (see Shaw, 2000), where melt is not completely extracted from the source so that the residue also includes a liquid phase. In this model, the melt retained in the porosity is in equilibrium with the last composition of the residual assemblage. We adopted the formulation of Zou (1998) for non-modal dynamic melting, where **Φ**, the critical mass porosity (cmp), represents the minimum porosity necessary to reach interconnection among melt pockets to allow melt migration. At the same time it represents the residual porosity after melt extraction. If $F$ is the degree of melting, and $X$ is the extracted melt fraction, we have $X = F - \mathbf{\Phi}$ (Zou, 1998).

Figure 7 shows the results for Ti–Zr modelling of cpx compositions for dynamic (non-modal) melting with variable cmp. We evaluated separately the effects of the cmp in the spinel and garnet stability fields. Variation of the cmp parameter in the spinel field leads to a change of the melting slope (Fig. 7a). A cmp variation of the same order, for melting starting in the garnet field, has a weaker effect (Fig. 7b). The overall melting path is mainly governed by the spinel field cmp (Fig. 7c). The model paths become subparallel to the measured trends at cmp ≥0·01. One predicted effect of increasing cmp is to progressively enrich Ti and Zr in the residue at the clinopyroxene-out limit ($F \approx 25\%$, Fig. 7c). This limit, however, moves as a function of the degree of melting in the garnet field because of the highest consumption of clinopyroxene during melting in the garnet stability field (Fig. 7d). With melting modes used in this model (see Appendix) total $F$ at the clinopyroxene-out limit shortens by ∼0·8% when garnet melting increases by 1%.

The effect of variable cmp on the REE melting paths is indicated in Fig. 8. Variation of the cmp in the spinel field has the effect of modifying the slope of the melting paths (Fig. 8a). Model melting paths are far from the measured MREE and HREE trends at high cmp values. The effect of varying cmp in the garnet field is weaker than that observed in the spinel field; however, it significantly enhances LREE buffering with respect to the MREE and HREE (Fig. 8b and c). A constant cmp along the entire melting path (Fig. 8a) approaches a simultaneous match of the REE ratios better than a fractional model because melting in the garnet field shifts the spinel melting paths above the measured values (compare with Fig. 6). For a given sample, however, cmp and degree of melting in the garnet field vary



Downloaded from http://petrology.oxfordjournals.org/ at Kainan University on March 17, 2015

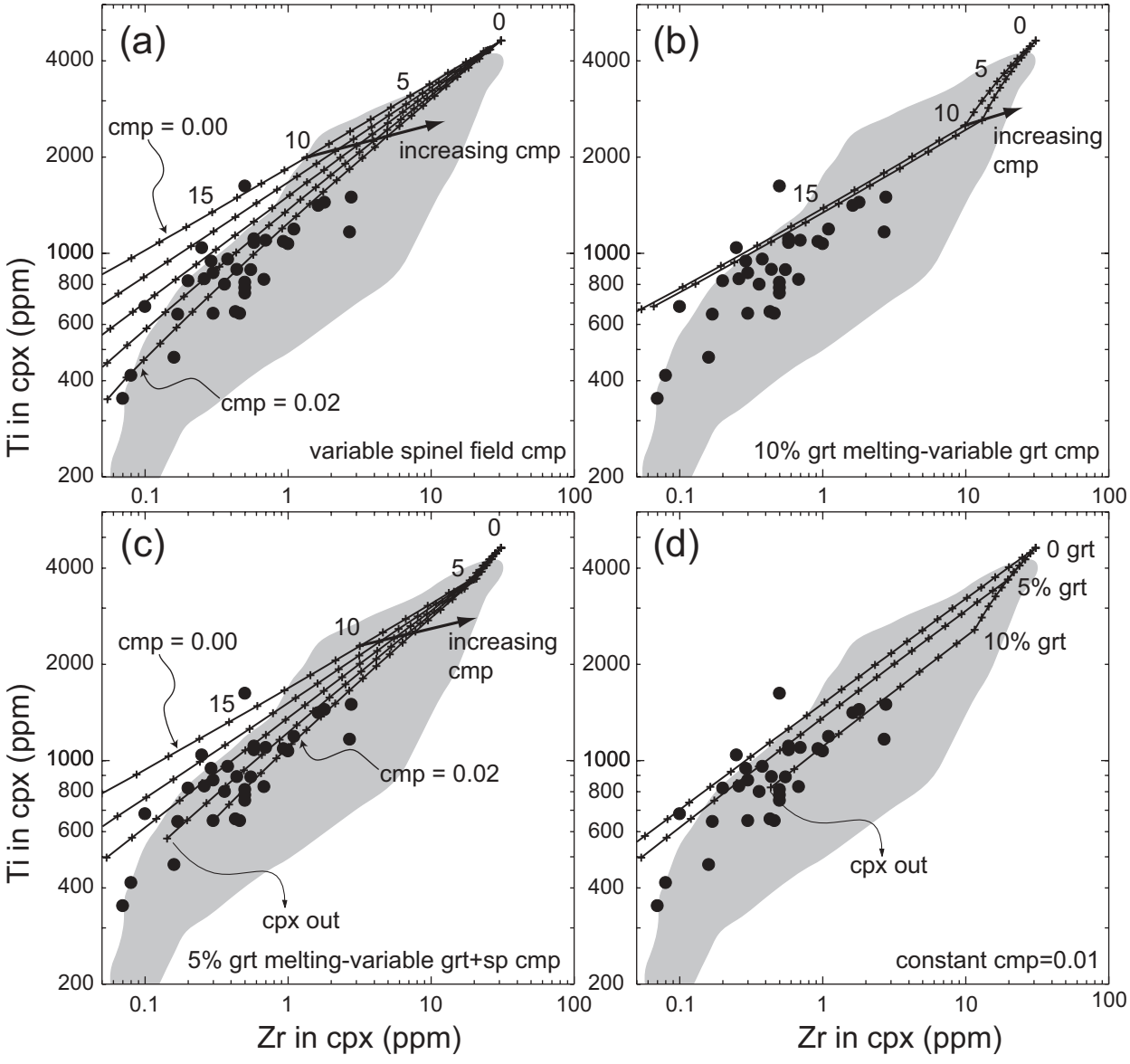


**Fig. 7.** Model melting paths varying the critical mass porosity (cmp) in a dynamic (non-modal) melting scenario. (a) Variation of the cmp in the spinel field. Cmp increases from 0·00 (= fractional) to 0·02. The arrow shows the direction of increasing cmp. (b) Variation of the cmp in the garnet field only. Both curves refer to 10% garnet dynamic (non-modal) melting followed by fractional non-modal melting in the spinel field. Garnet field cmp are 0·00 and 0·02, increasing in the direction of the arrow. (c) Variation of the cmp in both garnet and spinel fields after melting 5% in the garnet field followed by melting in the spinel field. Arrows show the direction of increasing cmp [cmp values are the same as in (a)]. (d) Vema Lithospheric Section samples and global dataset compared with curves of non-modal dynamic melting in the garnet (variable) + spinel fields at a fixed 0·01 cmp. Tick marks are 1% melting steps.

strongly if estimated on the basis of LREE, MREE or HREE ratios. This appears clearly in Fig. 8d where, for instance, melting in the range 0–5% in the garnet stability field brackets ~15, 25 and 50% of the plotted data for $Dy/Yb_{(N)}$, $Sm/Yb_{(N)}$ and $Ce/Yb_{(N)}$, respectively. Similar considerations can be extended to the cmp variation (Fig. 8c).

Element diffusion during melting can explain LREE enrichment (Van Orman *et al.*, 2002). Nevertheless, widespread interstitial mineral crystallization leads us to consider the effects of adding small amounts of partial and aggregated melts to the residual rocks, as discussed in the next section.

## Post-melting refertilization

The mechanism by which melt is extracted from the mantle is a hotly debated issue. The relatively homogeneous composition of erupted MORB magmas contrasts



Downloaded from http://petrology.oxfordjournals.org/ at Kainan University on March 17, 2015

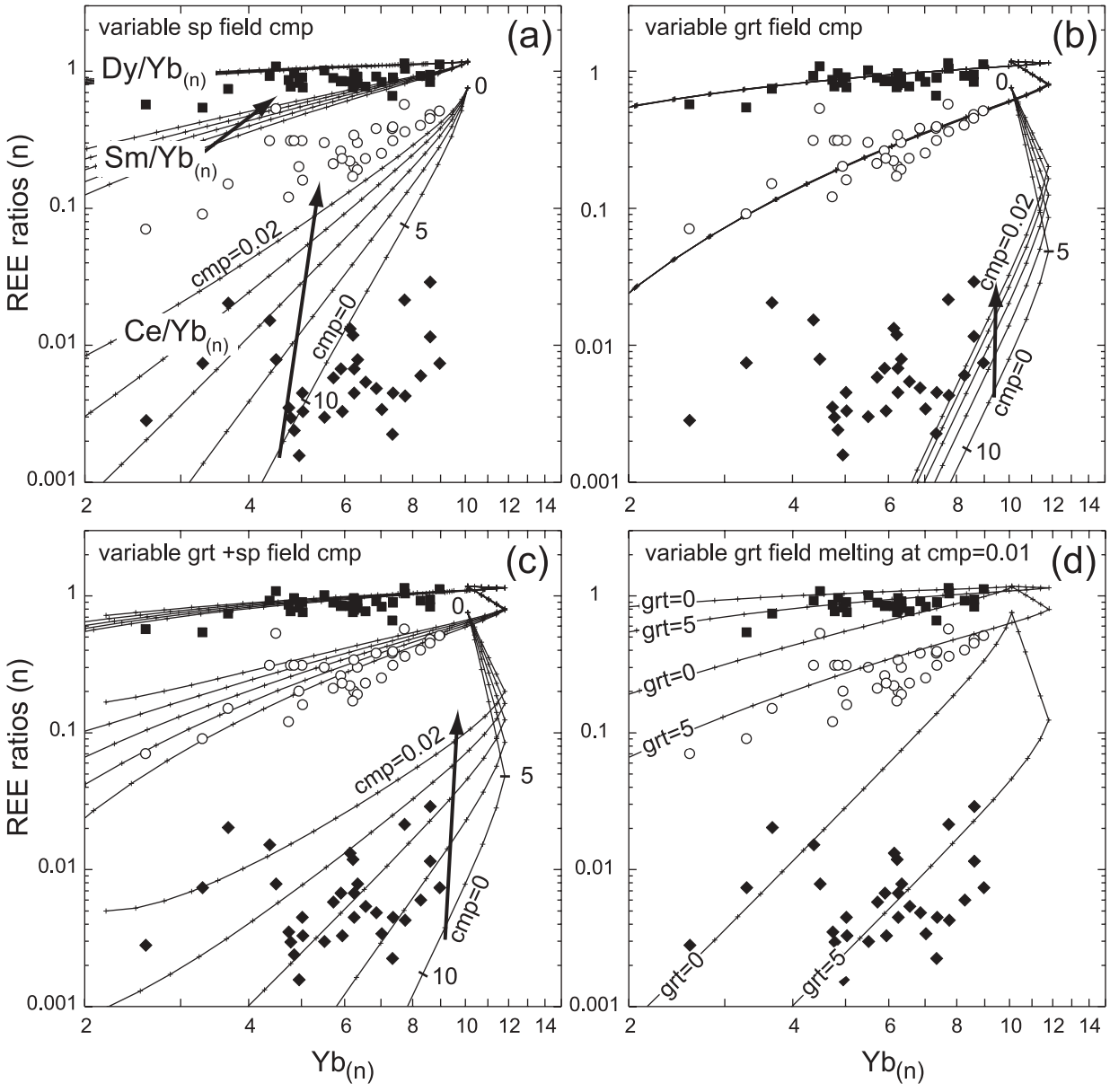


**Fig. 8.** Model dynamic (non-modal) melting paths varying the critical mass porosity (cmp) compared with the Vema Lithospheric Section clinopyroxene contents for $Dy/Yb_{(n)}$, $Sm/Yb_{(n)}$ and $Ce/Yb_{(n)}$ vs $Yb_{(n)}$ (symbols as in Fig. 6). (a) Variation of the cmp in the spinel field; the arrows show the direction of increasing cmp (from 0·00 = fractional to 0·005, 0·01, 0·015 and 0·02). (b) Variation of the cmp in the garnet field followed by fractional melting in the spinel field; cmp values are the same as in (a). (c) Variation of the cmp in both garnet and spinel fields for the same cmp values as in (a). (d) Dynamic melting paths (cmp = 0·01) with 0% (spinel field) and 5% garnet field melting. Tick marks represent 1% melting steps. Total extent of melting (5% increments) is reported for reference on the $Ce/Yb_{(n)}$ fractional (cmp = 0·00) melting path in (a), (b) and (c).

with the extreme heterogeneity of melt inclusions in olivine phenocrysts (Sobolev & Shimizu, 1993) or plagioclase (Sours-Page *et al.*, 1999), suggesting shallow mixing of compositionally different magma batches. Seyler *et al.* (2001) and Hellebrand *et al.* (2002) have found evidence that small (≤2%), heterogeneously distributed, quantities of transient melt have crystallized within residual peridotites. We have found similar textural evidence in the VLS residual peridotites, suggesting that crystallization of small amounts of melt is common in residual abyssal peridotites. As shown above, such microtextures are only partially attributable to crystallization under dynamic melting conditions, i.e. the liquids are in equilibrium with the last composition of the residual assemblage. Determining the out-of-equilibrium component of such liquids allows recognition of their nature, provenance and



Downloaded from http://petrology.oxfordjournals.org/ at Kainan University on March 17, 2015

spatial heterogeneity. The term refertilization is used here to emphasize that melts are not in equilibrium (too enriched) with the residual composition to which they are added. They differ substantially from melts retained in the residual porosity during melting, as these only buffer the incompatible element content during melting and do not refertilize *sensu stricto*.

We have addressed this problem by testing refertilization with variably aggregated melts in order to recognize the source region and degree of aggregation of partial melts percolating through the mantle rocks. Compositional end-members are represented by instantaneous and aggregated melts. After considering the effects of both end-members on variably depleted mantle assemblages, we attempt to evaluate, case by case, the aggregation interval necessary for a partially aggregated melt to reproduce the measured residual clinopyroxene REE patterns by refertilization of a variably depleted residual mantle.

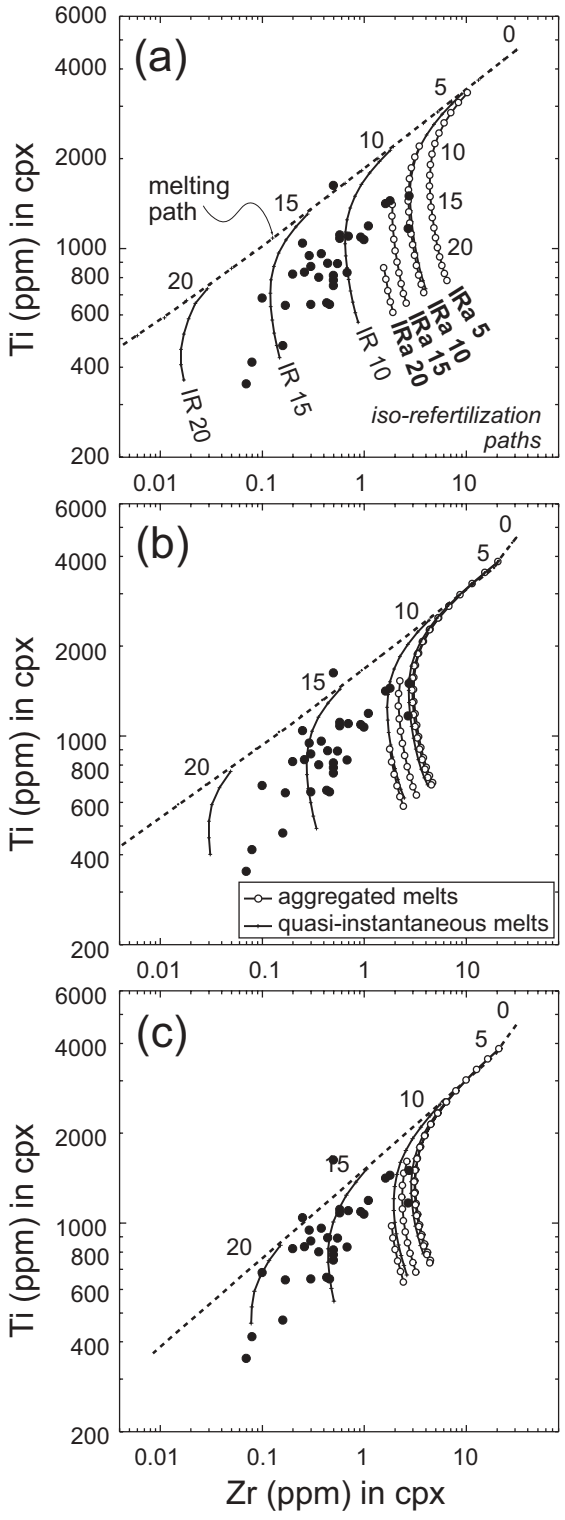


**Fig. 9.** Ti–Zr relationships in clinopyroxene compared with model iso-refertilization paths. Each path shows how the composition of a variably depleted clinopyroxene is modified by adding a constant amount of melt to the depleted peridotite. The composition of a residual clinopyroxene stays on an iso-refertilization path when quasi-instantaneous (continuous lines, small ticks) or variably aggregated (continuous lines, open circles) melts are added back to the rock. Plotted here are the cases in which melts extracted after 5, 10, 15 and 20% source partial melting are added to a variably depleted, purely residual, peridotite (IR *x*, compositional paths followed by a variably depleted residual clinopyroxene refertilized with a quasi-instantaneous melt extracted after *x* *F*% source partial melting; **IRa *x***, iso-refertilization paths when refertilization is made by melts aggregated from the base to $F = x$). The unmodified evolution of a residual clinopyroxene following the melting path is shown for reference (dashed line). (a) Iso-refertilization paths adding 0·5% quasi-instantaneous and aggregated melts after non-modal fractional melting in the spinel field. (b) Iso-refertilization paths adding 0·5% quasi-instantaneous and aggregated melts after 5% non-modal fractional melting in the garnet field followed by melting in the spinel field. (c) Refertilization paths adding 0·5% quasi-instantaneous and aggregated melts after 5% dynamic melting in the garnet field followed by melting in the spinel field (cmp = 0·005 over the entire melting column).

## Refertilization with aggregated melts

Aggregated melts result from mixing of all the instantaneous components produced during progressive depletion of a mantle source. To evaluate the effects of a variably aggregated melt on the residual source, we calculate the composition of melts aggregated from the base of the melting column to total degrees of melting of 5, 10, 15 and 20%. Residual mantle compositions, calculated for degrees of depletion exceeding those of the extracted melts, were then refertilized with 0·5% of the calculated melt (Figs. 9 and 10) assuming the melt was crystallizing 0·7 ol + 0·3 cpx (Elthon, 1992). We assumed perfect rapid extraction; that is, the residue experiences neither reactive percolation nor diffusive fractionation. Figures 9 and 10 show how the composition of clinopyroxene in a depleted mantle parcel is affected by the addition of 0·5% of a variably aggregated melt. The resulting curves represent clinopyroxene 'iso-refertilization' paths, i.e. the compositional variation of progressively depleted mantle

Downloaded from http://petrology.oxfordjournals.org/ at Kainan University on March 17, 2015

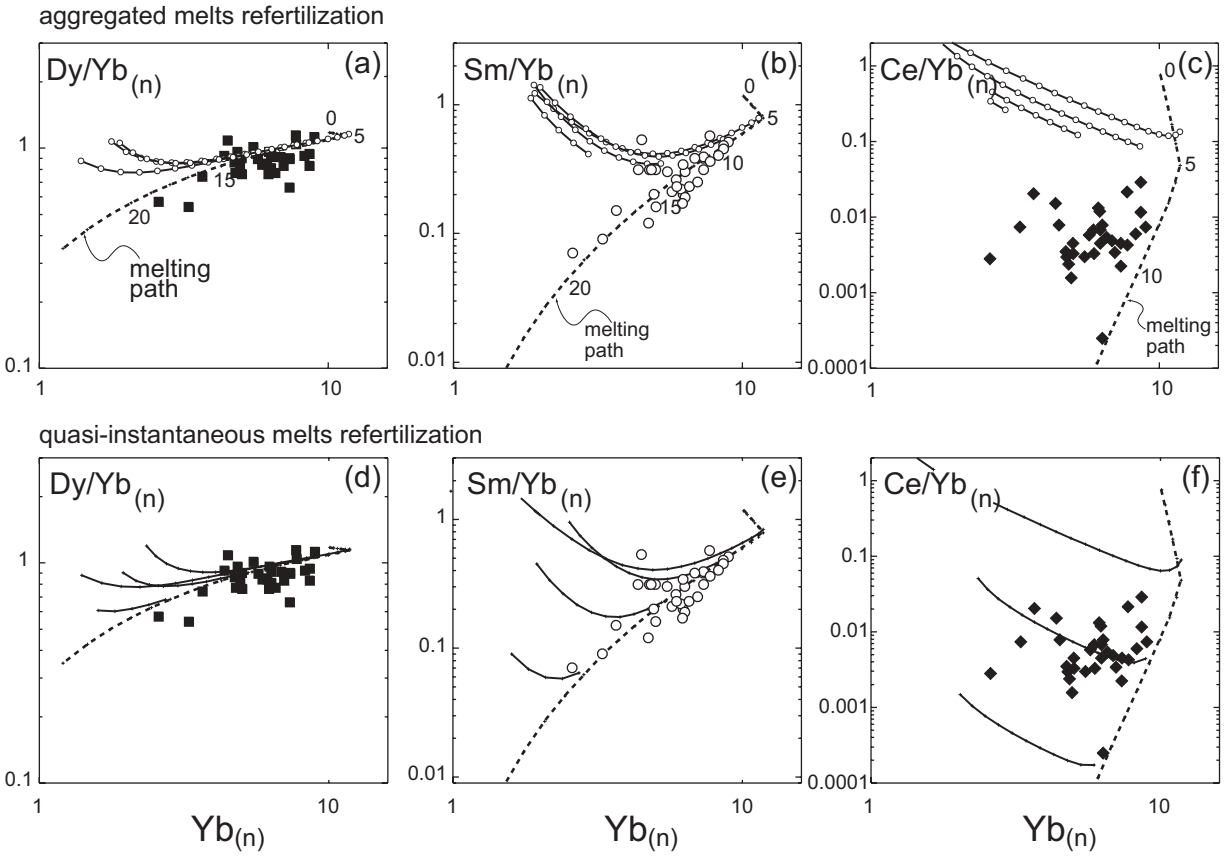


**Fig. 10.** $Dy/Yb_{(n)}$, $Sm/Yb_{(n)}$ and $Ce/Yb_{(n)}$ vs $Yb_{(n)}$ compared with model iso-refertilization paths for a residual peridotite-hosted clinopyroxene. Curves show how a variably aggregated (a–c) or quasi-instantaneous (d–f) melt can modify the clinopyroxene REE element contents after crystallizing 0·5% melt in a variably depleted source (see also caption to Fig. 9). All curves refer to 5% non-modal fractional melting in the garnet field followed by melting in the spinel field. Quasi-instantaneous (continuous lines, small ticks) and variably aggregated (continuous lines, open circles) melts are extracted after 5, 10, 15 and 20% source partial melting and added back to a rock that has undergone further melting. The composition of residual clinopyroxenes not affected by refertilization follows the normal melting path (dashed line).

parcels refertilized with a constant amount of melt aggregated over the same 'melting interval'.

Ti–Zr refertilization paths (open circles in Fig. 9) are calculated for: (1) non-modal fractional melting in the spinel field (Fig. 9a); (2) non-modal fractional melting in the spinel field after 5% in the garnet field (Fig. 9b); (3) with the same values as (2) for dynamic melting (Fig. 9c). Overall refertilization paths do not appear to be very sensitive to the melting mechanism, in so far as the composition of the aggregated (and partial) melt changes very little from a fractional to a dynamic model (Fig. 9b and c). Significantly, all paths resulting from refertilization with melts from 5 to 20% are shifted only slightly from each other because of the strong compositional control exerted by the first melt increments. Paths corresponding to refertilization with aggregated melts do not match the field of the VLS clinopyroxenes (Fig. 9).

REE iso-refertilization paths show that aggregated melts are too enriched in MREE and LREE with respect to the VLS clinopyroxenes (open circles in Fig. 10a–c). The over-enrichment is proportional to the incompatibility of each element.

## Refertilization with instantaneous melts

In a fractional melting model melts are extracted as soon as they are generated. As a result, successive instantaneous melt fractions extracted from the same source will be increasingly depleted. We explore the effects of refertilization with instantaneous melts using compositions corresponding to 1% melting steps (Fig. 11a), to avoid the problems related to very low degrees of melting (Baker *et al.*, 1995). Hereafter we will refer to these compositions as quasi-instantaneous melts. Iso-refertilization paths for Ti–Zr and REE (Figs 9 and 10) have been estimated for melts extracted after 5, 10, 15 and 20% source partial depletion. Refertilization by addition of quasi-instantaneous melts to rocks that have undergone degrees of melting ($F$) > 10% has a less drastic effect on the residual compositions than refertilization with the same amount of aggregated melts (Figs 9 and 10).



Downloaded from http://petrology.oxfordjournals.org/ at Kainan University on March 17, 2015

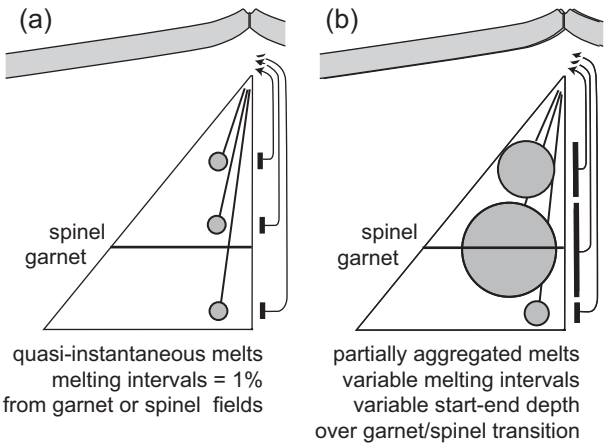


**Fig. 11.** Melt extraction and refertilization end-members used in this work: quasi-instantaneous melts (a) and partially aggregated melts (b) refertilize the source at the top of the melting column. Black bars represent the length of aggregation of the refertilizing melts; this is a rough approximation of the unknown extraction area (grey circles). Quasi-instantaneous melts result from 1% melting intervals (a). Partially aggregated melts are integrated over variable intervals (b); they may result from mixing quasi-instantaneous melts coming from both garnet and spinel fields.

The refertilization-induced enrichment is strongly controlled by the bulk *D*. The divergence between refertilization and melting paths increases toward the LREE, so that calculated refertilized compositions match the field of the VLS residual clinopyroxenes (Fig. 10; note that the scale increases from one to four log units from HREE to LREE). This suggests that interstitial clinopyroxene and spinel, interpreted as crystallization products of percolating melts, probably result from trapping quasi-instantaneous melts (or melts that are not aggregated over the whole melting column) rather than fully aggregated melts.

In general, irrespective of the variably aggregated or instantaneous nature of the melts, they always appear enriched in incompatible elements with respect to the source from which they come. Refertilization results in LREE and MREE enrichment relative to the HREE, i.e. slightly to markedly flatter REE patterns. When refertilization is taken into account, the amount of melting in the garnet field (responsible for Ce/Yb and Sm/Yb depletion) needs to be increased to partially balance the refertilization-induced over-enrichment necessary to match the whole REE patterns. In other words, if there is evidence of refertilization, melting in the garnet field becomes more and more important.

## Refertilization with partially aggregated melts

Refertilization paths with quasi-instantaneous melts are able to match the observed trace element enrichments. However, looking at each sample composition, it appears that refertilization with a quasi-instantaneous melt extracted from a given, variably depleted, source is not always able to exactly reproduce the observed patterns. To obtain a refertilizing melt with the correct composition it is normally necessary to mix quasi-instantaneous melts derived from a restricted interval within the melting column. We define these as partially aggregated melts; they are calculated by mixing equal parts of quasi-instantaneous melts derived from 1% melting steps (Fig. 11b; see Appendix). Intuitively, the degree of refertilization and degree of melting necessary to produce a particular trace element pattern are inversely correlated, i.e. the same pattern can be reproduced by adding greater amounts of melt and simultaneously increasing the degree of melting of the source. We have, therefore, estimated the minimum amount of melting and refertilization able to reproduce the observed patterns assuming a constant cmp all along the melting column (cmp = 0·005). Degrees of melting in the spinel and garnet field were set to the best fit with the observed REE patterns. Then the extent of the melting interval from which the melt was extracted and the degree of melting were adjusted iteratively searching for the minimum amount of refertilization.

The estimated degree of melting (garnet and spinel field), the amount of refertilization and melting interval from which the partial melts are extracted are reported in Table 8 and plotted in Fig. 12 for each VLS sample. Overall, it appears that the amount of melting in the garnet stability field is higher than expected for a slow-spreading scenario as in the VLS. The amount of partially aggregated melt required to equilibrate the pure residual pattern is generally low (0·1–1%). Refertilizing melts are aggregated over variable melting intervals (black bars in Fig. 12); they are derived from different depths and are never aggregated over the entire column. It is worth noting that melt components extracted from the garnet field are necessary to obtain the correct refertilizing melt composition. The overall suggestion is that quasi-instantaneous or partially aggregated melts are able to migrate to the top of the melting column rapidly and with a low degree of aggregation. The occurrence of melt batches rapidly extracted from discrete, small, parts of the melting region suggests that the extraction process is probably a discontinuous or episodic rather than a continuous steady-state process. Significantly, quasi-instantaneous melt components from the base of the melting column (within the garnet field) are detected less than those generated in the spinel field (Fig. 12). Deep melts, therefore, do not percolate through the residual rock, but are separated by transport through open channels (Nicolas, 1990) or dunite reactive channels (Kelemen *et al.*, 1995) or a combination of processes (Kelemen *et al.*, 1997; Dijkstra *et al.*, 2003). We conclude that the melting region undergoes discontinuous

Downloaded from http://petrology.oxfordjournals.org/ at Kainan University on March 17, 2015

*Table 8: Model melting parameters*

| Sample | *F*% | grt% | sp% | *R* (vol. %) | *A* (*F*%) | *B* (*F*%) |
|---|---|---|---|---|---|---|
| S1902-05 | 14·9 | 2·0 | 12·9 | 0·1 | 6·0 | 8·0 |
| S1903-05 | 19·1 | 12·1 | 7·0 | 0·3 | 11·1 | 12·1 |
| S1904-33 | 18·1 | 4·0 | 14·1 | 0·1 | 8·0 | 12·1 |
| S1904-42 | 16·1 | 5·0 | 11·1 | 0·1 | 7·0 | 11·1 |
| S1912-05 | 15·8 | 6·0 | 9·8 | 0·2 | 10·1 | |
| S1912-08 | 15·1 | 8·0 | 7·1 | 0·2 | 8·0 | 9·0 |
| S1913-03 | 11·1 | 6·0 | 5·1 | 0·3 | 9·0 | 10·1 |
| S1913-36 | 9·0 | 2·5 | 6·5 | 0·0 | | |
| S1920-84 | 12·0 | 5·7 | 6·3 | 0·1 | 4·7 | 7·7 |
| S1923-42 | 15·3 | 6·5 | 8·8 | 0·2 | 7·5 | 9·5 |
| S1923-45 | 18·1 | 8·0 | 10·1 | 0·0 | 8·0 | 9·0 |
| S1923-46 | 16·5 | 6·7 | 9·8 | 0·1 | 7·7 | 8·7 |
| S1924-01 | 18·1 | 12·1 | 6·0 | 0·8 | 9·0 | 10·1 |
| S1924-03 | 14·4 | 6·0 | 8·4 | 0·2 | 8·0 | 9·0 |
| S1924-04 | 13·1 | 6·0 | 7·1 | 0·1 | 7·0 | 9·0 |
| S1924-19 | 15·6 | 8·0 | 7·6 | 0·7 | 9·0 | 12·1 |
| S1925-56 | 12·8 | 1·0 | 11·8 | 0·1 | 8·0 | 9·0 |
| S1925-71 | 17·3 | 8·0 | 9·3 | 0·2 | 6·0 | 12·1 |
| S1927-01 | 18·3 | 10·1 | 8·2 | 0·2 | 9·0 | 11·1 |
| S1927-02 | 18·6 | 10·1 | 8·5 | 0·2 | 11·1 | 16·1 |
| S1927-05 | 18·1 | 10·1 | 8·0 | 0·2 | 9·0 | 10·1 |
| S1928-09 | 12·1 | 0·0 | 12·1 | 0·0 | | |
| S1930-79 | 20·4 | 7·0 | 13·4 | 0·1 | 7·0 | 10·1 |
| S2209-01 | 20·4 | 8·0 | 12·4 | 0·1 | 11·0 | 13·1 |
| S2220-06 | 17·9 | 7·5 | 10·4 | 0·2 | 7·5 | 10·6 |
| S2221-04 | 18·1 | 10·1 | 8·0 | 0·2 | 8·0 | 10·1 |
| S2221-05 | 19·3 | 11·1 | 8·2 | 0·2 | 11·1 | 14·1 |
| VE1-1 | 14·3 | 7·0 | 7·3 | 0·2 | 8·0 | 10·1 |
| VE1-5 | 14·6 | 3·0 | 11·6 | 0·1 | 8·0 | 13·6 |
| VE 4-7 | 16·6 | 7·0 | 9·6 | 0·2 | 9·0 | 13·1 |
| P7003-23-A | 23·1 | 11·1 | 12·0 | 0·1 | 13·1 | 22·1 |
| EW13-7 | 15·1 | 6·0 | 9·1 | 0·1 | 7·0 | 12·1 |
| EW16-1 | 14·5 | 2·9 | 11·6 | 0·0 | 9·0 | |
| EW16-5 | 16·6 | 8·5 | 8·1 | 0·2 | 8·5 | 13·6 |

*F*%, total degree of melting; grt% and sp%, degree of melting in the garnet and spinel field, respectively; *R*, amount of refertilization (vol. %); A and B, start and end point (*F*%) of the source of the refertilizing liquid referred to the base of the melting column.

processes where the onset of melting, porosity and melt extraction are heterogeneously distributed in space and time. Melt extraction appears to be a discontinuous or episodic process once it begins in the melting region. Compositional variations deriving from variable degrees of aggregation can be preserved until eruption, as shown by the extreme trace element variations in MORB from the Kolbeinsey Ridge by Devey *et al.* (1994). This observation also suggests that shallow mixing prior to eruption can be insufficient to hide the extraction-induced compositional variability.

## Source heterogeneity controls the onset of melting

Some key features of Fig. 12 help interpret the origin of the observed variations. An overall increase of the degree of melting from west (older) to east (younger) is accompanied by significant variability at the site scale.

Assuming that the garnet–spinel transition occurs at a constant depth, we can approximate the position of the melting column relative to the garnet–spinel transition by using the degree of melting in the garnet and spinel field as a proxy for the onset and final depths of melting. In Fig. 12 the base of the melting column deepens whereas the top rises with decreasing age of the crustal section. Such a variation can be generated by a general increase in mantle fertility and/or of mantle temperature. An increase of fertility results in a shift in the peridotite solidus toward lower temperatures, leading to a strong increase in the degree of melting in the garnet field and a negligible one in the spinel field. The peridotite solidus impacts a steep (adiabatic) mantle thermal gradient at the onset of melting, so any small variation in the solidus position results in large variations in the position of the base of the melting column (degree of melting in the garnet field). On the contrary, at the end of melting the *P*–*T* path of the mantle and the peridotite solidus cross at a high angle; therefore, even large shifts in the solidus position result in small displacements of the top of the melting column, i.e. in the amount of melting in the spinel field. On the other hand, a continuous increase of mantle temperature results in an increase in the degree of melting both in the garnet and spinel fields, either by shallowing the mantle isotherms or by deepening the garnet–spinel transition (Klemme & O'Neill, 2000). This is in line with the interpretation of Bonatti *et al.* (2003) based on gravity and compositional data.

To discuss the site-scale variability we focus particularly on the 10 sites from which more than one sample was analyzed. Seven out of the 10 sites show variability in the amount of melting in the garnet field greater than that in the spinel field. We propose that the origin of this variability stems from metre- (even sub-metre) scale compositional (modal) heterogeneity of the mantle source. Small-scale heterogeneities in the mantle exposed along the VLS were also detected in the Nd isotopic composition of clinopyroxene separated from the VLS peridotites; this contrasts with the >20 Myr nearly constant isotopic composition of the associated basaltic glasses (Cipriani *et al.*, 2004). The $^{143}Nd/^{144}Nd$ of the clinopyroxenes correlates weakly with the degree of melting undergone by the peridotite, calculated from the Cr-number of the residual mineral phases. This correlation

Downloaded from http://petrology.oxfordjournals.org/ at Kainan University on March 17, 2015

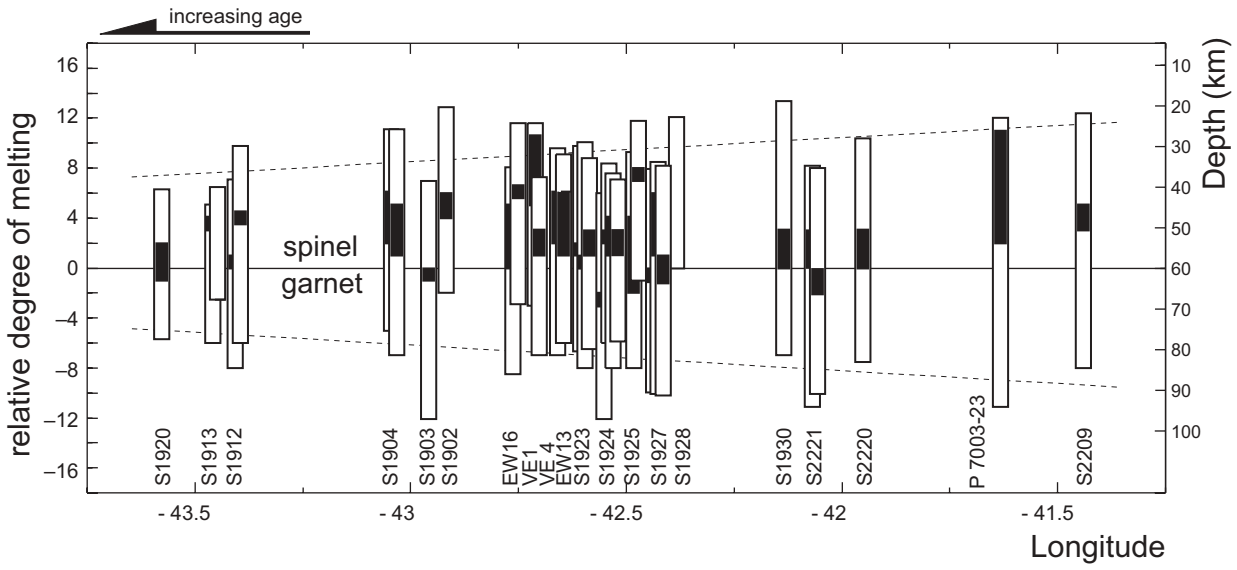


**Fig. 12.** Variation in the degree of melting and refertilization along the Vema Lithospheric Section estimated on the basis of the REE distribution in residual clinopyroxene. The length of each column (white bars) is proportional to the total amount of melting for a given sample plotted with respect to the garnet–spinel transition. Black bars show the region from which refertilizing melts are extracted and aggregated. All values are reported in Table 8. Dashed lines are linear regressions of the garnet- and spinel-field degrees of melting. The depth scale is calculated assuming the garnet–spinel transition is at 60 km depth and a melt productivity of 1%/kbar.

may suggest that the chemical composition of the mantle source records a depletion event that took place long before extraction of Vema MORB. The lack of correlation of the Nd isotopic composition with the Sm/Nd ratio, however, calls for possible refertilization of the source prior to melting (Cipriani *et al.*, 2004). Heterogeneities of such small amplitude may result from diffusive re-equilibration or crystallization/dissolution of orthopyroxene as a result of reactive percolation of silica-saturated/unsaturated pyroxenitic early melts (Salters & Dick, 2002; Kogiso *et al.*, 2004, and references therein). On the other hand, pyroxenitic melts are not required to explain the isotopic composition of VLS basalts (Cipriani *et al.*, 2004). However, reactions of pyroxenitic melts with the peridotite prior to melting could have contributed to the observed heterogeneities, as shown by the variable Nd isotopic composition of the clinopyroxenes within single dredge hauls. We are not able at this stage to determine the nature of the melts responsible for the pristine refertilization of the VLS peridotites but they must result in compositional (modal) heterogeneity. Modal inhomogeneity leads to a punctuated initiation of melting driven by the distribution of the more fusible phases (Luth, 2002), and, thus, to a heterogeneous distribution of porosity. The cmp can be locally exceeded, generating variability in the REE-inferred degree of melting. Significantly, the scatter in the amount of garnet-field melting is stronger than that observed in the spinel field. This may result from reduction of the heterogeneities during ascent. If heterogeneities, and, therefore, melt distribution are going to be reduced as partial melting progresses, we expect the amount of melting in the spinel field to be less variable than that in the garnet field. This is observed along the VLS (Fig. 12) where the overall variability of degree of melting in the spinel field ($1\sigma = 2{\cdot}1$) is less than that inferred for the garnet field ($1\sigma = 3{\cdot}0$).

## CONCLUSIONS

(1) VLS peridotites are residual after 9–23% partial melting with a variable amount of melting in the garnet field estimated on the basis of the REE contents of clinopyroxene.

(2) In a dynamic melting scenario, the behaviour of trace elements such as Ti–Zr and REE depends strongly on the residual porosity during melting. Residual porosity and estimated amount of melting are interdependent, so that the porosity profile in the melting column is a key factor in evaluating the degree of melting undergone by a mantle parcel.

(3) Modelling the REE patterns of the VLS residual clinopyroxene reveals a stronger than expected extent of melting in the garnet field. The variability of the amount of melting in the garnet field, compared with that in the spinel field, suggests that the onset of melting is heterogeneous at small (less than metre) scale, possibly as a result of modal heterogeneity of the source.

(4) REE and Ti–Zr in residual clinopyroxene suggest a weak refertilization of the source by small (0·1–1%)



Downloaded from http://petrology.oxfordjournals.org/ at Kainan University on March 17, 2015

amounts of melt derived from different depths in the melting column. The refertilizing melts have a trace element composition corresponding to that of quasi-instantaneous or partially aggregated melts, often including a garnet-field derived component.

(5) Refertilizing partial melts trapped in the source are mostly from the upper part of the melting region, suggesting that at the top of the melting column only the deeper (garnet-field) melts are well separated from the source by focused transport mechanisms, and do not affect the composition of the percolating melts.

(6) The lower and upper expansion of the estimated melting column moving toward younger ages suggests that mantle temperature beneath this sector of the Mid-Atlantic Ridge has increased steadily during the last 20 Myr.

## ACKNOWLEDGEMENTS

We acknowledge the invaluable work of the crew, officers and scientific party of the two *A. N. Strakhov* expeditions in 1998 and 2000. The original manuscript was greatly improved by reviews and discussion with Eric Hellebrand, Colin Devey, Kevin Johnson and two anonymous reviewers. D.B. is grateful to Robert Clocchiatti for his precious continuous support and to Catherine Mevel for hosting at the Laboratoire de Géosciences Marines (IPGP) during his Ph.D. We also acknowledge the helpful contributions by M. Ligi and M. Treuil. This work has been supported by the Italian Consiglio Nazionale Ricerche (Progetto Strategico Dorsali) and the US National Science Fundation (OCE-9911753; OCE-0328217). D.B. acknowledges the financial support provided through the European Community's Human Potential Program under contract HPRN-CT-2002-000211 [EUROMELT]. This is ISMAR-CNR Contribution 1452 and Lamont Doherty Contribution LDEO 6794.

## REFERENCES

Anders, E. & Grevesse, N. (1989). Abundances of the elements: meteoritic and solar. *Geochimica et Cosmochimica Acta* **53**, 197.

Auzende, J. M., Bideau, D., Bonatti, E., Cannat, M., Honnorez, J., Lagabrielle, Y., Malavieille, J., Mamaloukas-Frangoulis, V. & Mevel, C. (1989). Direct observation of a section through slow-spreading oceanic crust. *Nature* **337**, 726–729.

Baker, M. B., Hirschmann, M. M., Ghiorso, M. S. & Stolper, E. M. (1995). Compositions of near-solidus peridotite melts from experiments and thermodynamic calculations. *Nature* **375**, 308–311.

Bence, A. E. & Albee, A. L. (1968). Empirical correction factors for the electron microanalyses of silicates and oxides. *Journal of Geology* **76**, 382–403.

Blundy, J., Robinson, J. A. C. & Wood, B. (1998). Heavy REE are compatible in clinopyroxene on the spinel lherzolite solidus. *Earth and Planetary Science Letters* **160**, 493–504.

Bonatti, E., Seyler, M. & Sushevskaya, N. (1993). A cold suboceanic mantle belt at the Earth's equator. *Science* **261**, 315–320.

Bonatti, E., Ligi, M., Brunelli, D., Cipriani, A., Fabretti, P., Ferrante, V., Gasperini, L. & Ottolini, L. (2003). Mantle thermal pulses below the Mid-Atlantic Ridge and temporal variations in the formation of oceanic lithosphere. *Nature* **423**, 499–505.

Bonatti, E., Brunelli, D., Buck, W. R., Cipriani, A., Fabretti, P., Ferrante, V., Gasperini, L. & Ligi, M. (2006). Flexural uplift of a lithospheric slab near the Vema Transform (Central Atlantic): timing and mechanisms. *Earth and Planetary Science Letters* **240**, 642–655.

Bottazzi, P., Ottolini, L. & Vannucci, R. (1990). Quantitative SIMS analysis of rare earth elements in mafic–ultramafic rock samples. In: *Proceedings of the Seventh International Conference on Secondary Ion Mass Spectrometry SIMS VII*. Chichester: John Wiley, pp. 413–416.

Bottazzi, P., Ottolini, L., Vannucci, R. & Zanetti, A. (1994). An accurate procedure for the quantification of rare elements in silicates. In: *Proceedings of the Ninth International Conference on Secondary Ion Mass Spectrometry SIMS IX*. Chichester: John Wiley, pp. 927–930.

Brunelli, D., Cipriani, A., Ottolini, L., Peyve, A. & Bonatti, E. (2003). Mantle peridotites from the Bouvet Triple Junction Region, South Atlantic. *Terra Nova* **15**, 194–203.

Cande, S. C., LaBreque, J. L. & Haxby, W. F. (1988). Plate kinematics of the South Atlantic, chron C34 to the present. *Journal of Geophysical Research* **93**, 13479–13492.

Cannat, M. & Seyler, M. (1995). Transform tectonics, metamorphic plagioclase and amphibolitization in ultramafic rocks of the Vema transform fault (Atlantic Ocean). *Earth and Planetary Science Letters* **133**, 283–298.

Cannat, M., Mamaloukas-Frangulis, V., Auzende, J.-M., Bideau, D., Bonatti, E., Honnorez, J., Lagabrielle, Y., Malavieille, J. & Mevel, C. (1991). A geological cross-section of the Vema fracture zone transverse ridge, Atlantic Ocean. *Journal of Geodynamics* **13**, 97–118.

Cipriani, A., Brueckner, H. K., Bonatti, E. & Brunelli, D. (2004). Oceanic crust generated by elusive parents: Sr and Nd isotopes in basalt–peridotite pairs from the Mid-Atlantic Ridge. *Geology* **32**, 657–660.

Devey, C. W., Garbe-Schönberg, C.-D., Stoffers, P., Chauvel, C. & Mertz, D. F. (1994). Geochemical effects of dynamic melting beneath ridges: reconciling major and trace element variations in Kolbeinsey (and global) mid-ocean ridge basalt. *Journal of Geophysical Research* **99**, 9077–9095.

Dick, H. J. B. (1989). Abyssal peridotites, very slow spreading ridges and ocean ridge magmatism. In: Saunders, A. D. & Norry, M. J. (eds) *Magmatism in the Ocean Basins. Geological Society, London, Special Publications* **42**, 71–105.

Dick, H. J. B. & Bullen, T. (1984). Chromian spinel as a petrogenetic indicator in abyssal and alpine-type peridotites and spatially associated lavas. *Contributions to Mineralogy and Petrology* **86**, 54–76.

Dijkstra, A. H., Barth, M. G., Drury, M. R., Mason, P. R. D. & Visser, R. L. M. (2003). Diffuse porous melt flow and melt–rock reaction in the mantle lithosphere at a slow-spreading ridge: a structural petrology and LA-ICP-MS study of the Othris Peridotite Massif (Greece). *Geochemistry, Geophysics, Geosystems* **4**(8613), doi: 10.1029/2001GC000278.

Dosso, L., Bougault, H., Schilling, J. G. & Joron, J.-L. (1991). Sr–Nd–Pb geochemical morphology between 10° and 17°N on the Mid-Atlantic Ridge: a new MORB isotope signature. *Earth and Planetary Science Letters* **106**, 29–43.

Dosso, L., Bougault, H. & Joron, J. L. (1993). Geochemical morphology of the north Mid-Atlantic Ridge, 10°–24°N, trace element–isotope complementarity. *Earth and Planetary Science Letters* **120**, 443–462.

Downloaded from http://petrology.oxfordjournals.org/ at Kainan University on March 17, 2015

Elthon, D. (1992). Chemical trends in abyssal peridotites; refertilization of depleted suboceanic mantle. *Journal of Geophysical Research* **97**, 9015–9025.

Faul, U. H. (2001). Melt retention and segregation beneath mid-ocean ridges. *Nature* **410**, 920–923.

Forsyth, D. W., Scheirer, D. S., Webb, S. C., Dorman, L. M., Orcutt, J. A., Harding, A. J., Blackman, D. K., Morgan, J. P., Detrick, R. S., Shen, Y., Wolfe, C. J., Canales, J. P., Toomey, D. R., Sheehan, A. F., Solomon, S. C. & Wilcock, W. S. D. (1998). Imaging the deep seismic structure beneath a mid-ocean ridge: the MELT Experiment. *Science* **280**, 1215–1218.

Ghose, I., Cannat, M. & Seyler, M. (1996). Transform fault effect on mantle melting in the MARK area (Mid-Atlantic Ridge south of the Kane transform). *Geology* **24**, 1139–1142.

Hellebrand, E., Snow, E. J., Dick, H. J. B. & Hofman, A. W. (2001). Coupled major and trace-element melting indicators in mid-ocean ridge peridotites. *Nature* **410**, 677–681.

Hellebrand, E. & Snow, J. E. (2003). Deep melting and sodic metasomatism underneath the highly oblique-spreading Lena Trough (Arctic Ocean). *Earth and Planetary Science Letters* **216**, 283–299.

Hellebrand, E., Snow, J. E., Hoppe, P. & Hofman, A. W. (2002). Garnet-field melting and late-stage refertilization in 'residual' abyssal peridotites from the Central Indian Ridge. *Journal of Petrology* **43**, 2305–2338.

Johnson, K. T. M. (1998). Experimental determination of partition coefficients for rare-earth and high-field-strength elements between clinopyroxene, garnet and basaltic melt at high pressures. *Contributions to Mineralogy and Petrology* **133**, 60–68.

Johnson, K. T. M. & Dick, H. J. B. (1992). Open system melting and spatial variation of peridotite and basalt at the Atlantis II Fracture Zone. *Journal of Geophysical Research* **97**, 9219–9241.

Johnson, K. T. M., Dick, H. J. B. & Shimizu, N. (1990). Melting in the oceanic upper mantle: an ion microprobe study of diopsides in abyssal peridotites. *Journal of Geophysical Research* **95**, 2661–2678.

Kelemen, P. B., Whitehead, J. A., Aharanov, E. & Jordhal, K. A. (1995). Experiments on flow focusing in soluble porous media, with applications to melt extraction from the mantle. *Journal of Geophysical Research* **100**, 475–496.

Kelemen, P. B., Hirth, G., Shimizu, N., Spiegelman, M. & Dick, H. J. B. (1997). A review of melt migration processes in the adiabatically upwelling mantle beneath oceanic spreading ridges. *Philosophical Transactions of the Royal Society of London, Series A* **355**, 283–318.

Kinzler, R. J. (1997). Melting of mantle peridotites at pressure approaching the spinel to garnet transition: application to mid ocean ridge basalt petrogenesis. *Journal of Geophysical Research* **102**, 953–974.

Klemme, S. & O'Neill, H. St. C. (2000). The near-solidus transition from garnet lherzolite to spinel-lherzolite: experiments in the system $CaO–MgO–Al_2O_3–SiO_2$. *Contributions to Mineralogy and Petrology* **138**, 237–248.

Kogiso, T., Hirschmann, M. M. & Reiners, P. (2004). Length scale of mantle heterogeneities and their relationship to ocean island basalt geochemistry. *Geochimica et Cosmochimica Acta* **68**, 345–360.

Luth, R. W. (2002). Possible implications of modal mineralogy for melting in mantle lherzolites. *Geochimica et Cosmochimica Acta* **66**, 2091–2098.

Michael, P. J. & Bonatti, E. (1985). Peridotite composition from the North Atlantic: regional and tectonic variations and implications for partial melting. *Earth and Planetary Science Letters* **73**, 91–104.

Nicolas, A. (1990). Melt extraction from mantle peridotites: hydrofracturing and porous flow, with consequences for oceanic ridge activity. In: Ryan, M. P. (ed.) *Magma Transport and Storage*. New York: John Wiley, pp. 159–174.

Rampone, E., Bottazzi, P. & Ottolini, L. (1991). Complementary Ti and Zr anomalies in orthopyroxene and clinopyroxene from mantle peridotites. *Nature* **354**, 518–520.

Ross, K. & Elthon, D. (1997). Extreme incompatible trace-element depletion of diopside in residual mantle from south of the Kane Fracture Zone. In: Karson, J. A., Cannat, M., Miller, D. J. & Elthon, D. (eds) *Proceedings of the Ocean Drilling Program, Scientific Results, 153*. College Station, TX: Ocean Drilling Program, pp. 277–284.

Salters, V. J. M & Dick, H. J. B. (2002). Mineralogy of the mid-ocean-ridge basalt source from neodymium isotopic composition of abyssal peridotites. *Nature* **418**, 68–72.

Seyler, M. & Bonatti, E. (1997). Regional-scale melt–rock interaction in lherzolitic mantle in the Romanche Fracture Zone (Atlantic Ocean). *Earth and Planetary Science Letters* **146**, 273–287.

Seyler, M., Toplis, M., Lorand, J. P., Luguet, A. & Cannat, M. (2001). Clinopyroxene microtextures reveal incompletely extracted melts in abyssal peridotites. *Geology* **29**, 155–158.

Seyler, M., Cannat, M. & Mével, C. (2003). Evidence for major-element heterogeneity in the mantle source of abyssal peridotites from the Southwest Indian Ridge (52° to 68°E). *Geochemistry, Geophysics, Geosystems* **4**(9101), doi:10.1029/2002GC000305.

Shaw, D. M. (2000). Continuous (dynamic) melting theory revisited. *Canadian Mineralogist* **38**, 1041–1063.

Sobolev, A. V. & Shimizu, N. (1993). Ultra-depleted primary melt inclusions in an olivine from the Mid-Atlantic Ridge. *Nature* **363**, 151–154.

Sours-Page, R., Johnson, K. T. M., Nielsen, R. L. & Karsten, J. L. (1999). Local and regional variation in MORB parental magmas: evidence from melt inclusions from the Endeavor segment of the Juan da Fuca Ridge. *Contributions to Mineralogy and Petrology* **134**, 342–363.

Suhr, G., Seck, H. A., Shimizu, N., Günther, D. & Jenner, G. (1998). Infiltration of refractory melts into the lowermost oceanic crust: evidence from dunite- and gabbro-hosted clinopyroxenes in the Bay of Islands Ophiolite. *Contributions to Mineralogy and Petrology* **131**, 136–154.

Vaggelli, G., Olmi, F. & Ponticelli, S. (1999). Quantitative electron microprobe analysis of reference silicate mineral and glass samples. *Acta Vulcanologica* **11**, 297–303.

Van Orman, J. A., Grove, T. L. & Shimizu, N. (2002). Diffusive fractionation of trace elements during production and transport of melt in Earth's upper mantle. *Earth and Planetary Science Letters* **198**, 93–112.

Walter, M. J. (1998). Melting of garnet peridotite and the origin of komatiite and depleted lithosphere. *Journal of Petrology* **39**, 29–60.

Zou, H. (1998). Trace element fractionation during modal and non-modal dynamic melting and open-system melting: a mathematical treatment. *Geochimica et Cosmochimica Acta* **62**, 1937–1945.

## APPENDIX

To calculate the compositional evolution of a trace element in a partial melting residue we used a stepwise calculation procedure. For each step we calculate the composition of the bulk residue, residual phases and extracted melt. Bulk distribution coefficients, melting and residual modes were calculated for each step.

### Governing equations

Trace element compositions have been calculated for the residue and the extracted melt following the formulation of Zou (1998).

Downloaded from http://petrology.oxfordjournals.org/ at Kainan University on March 17, 2015

A general expression can be used for both fractional and dynamic non-modal melting by changing the governing parameters. In a dynamic melting scenario the residual assemblage also includes a liquid phase. The concentration of a trace element in the residual assemblage is given by

$$C_{\mathrm{res}} = C_0 \frac{1}{1-X}\left\{1 - \frac{X[P+\Phi(1-P)]}{D_0+\Phi(1-P)}\right\}^{1/[\Phi+(1-\Phi)P]} \tag{A1}$$

where

$C_{\mathrm{res}}$ is the concentration of a trace element in the residue (residual solid + residual melt);

$C_0$ is the concentration of a trace element in the source;

$P$ is weighted liquid partition coefficient: $P = \sum kd^{i/l} p^i$, where $p^i$ is the melting mode of the phase $i$;

$D_0$ is the initial bulk distribution coefficient of the source: $D_0 = \sum Kd^{i/l} X_{0,i}$, where $X_{0,i}$ is the mode of the phase $i$ in the source;

$\Phi$ is critical mass porosity, i.e. the minimum 'critical' amount of partial melting required to allow segregation of the melt from the source; this also represents the amount of melt retained in the source after extraction;

$X$ is the fraction of extracted melt; this is related to $F$ (total degree of melting undergone by the source) and to the critical mass porosity $\Phi$ by

$$X = 0 \quad \text{for } F \leq \Phi$$
$$X = \frac{F-\Phi}{1-\Phi} \quad \text{for } F > \Phi.$$

Critical mass porosity is related to the volume porosity $\phi$ by the relation

$$\Phi = \frac{\rho_f \phi}{\rho_f \phi + \rho_s(1-\phi)}$$

where $\rho_f$ is the density of the melt and $\rho_s$ is the density of the residue.

The relative concentration of a trace element in the extracted liquid is given by

$$C_{\mathrm{res}} = \frac{C_0}{X}\left\{1 - \left[1 - \frac{X[P+\Phi(1-P)]}{D_0+\Phi(1-P)}\right]^{1/[\Phi+(1-\Phi)P]}\right\}. \tag{A2}$$

Fractional (non-modal) melting represents the particular case in which there is no residual porosity ($\Phi = 0$), i.e. all the melt is perfectly extracted from the source ($X = F$). By setting $\Phi = 0$ equations (A1) and (A2) become the fractional melting equations of Shaw (1970). Modal melting corresponds to the particular case in which $P = D_0$.

## Partition coefficients, initial and melting mode

We adopted the source composition, partition coefficient and mineral mode datasets used by Hellebrand *et al.* (2002), except for Ti content, which was set to be 0·22% in the source (Table A1). Partition coefficients were compiled based on Blundy *et al.* (1998) and Suhr *et al.* (1998), with the exception of Gd obtained by averaging adjacent element values. Initial and melting modes are from Johnson *et al.* (1990), Kinzler (1997), Johnson (1998) and Walter (1998). We also adopted a variable $D$ model to account for HREE compatibility at high pressure on the basis of the data of Blundy *et al.* (1998) and Hellebrand *et al.* (2002).

Measured clinopyroxene contents relate to mantle peridotites equilibrated in the spinel field. Thus, we recalculate model trends for spinel-field equilibrated assemblages to make them directly comparable with measured values assuming an instantaneous garnet–spinel transition according to the following reaction (Johnson *et al.*, 1990):

$$1{\cdot}0\ \mathrm{Ol} + 1{\cdot}0\ \mathrm{Gt} = 2{\cdot}5\ \mathrm{Opx} + 1{\cdot}0\ \mathrm{Sp} + 0{\cdot}75\ \mathrm{Cpx}.$$

## Refertilization

Refertilization has been calculated by adding back to the source a small (variable) amount of melt extracted after a variable extent of partial melting undergone by the source. The composition of a quasi-instantaneous melt was calculated using equation (A2) for $X = 0{\cdot}01$ from a variably depleted source. The composition of partially aggregated melts is the average of the individual quasi-instantaneous melts weighted by their amount, for simplicity assuming constant productivity and equal mixing:

$$C_{\mathrm{ref}} = \frac{\sum_{n=a}^{n=b} C_n}{b-a}$$

where $C_{\mathrm{ref}}$ is the composition of the refertilizing partially aggregated melt; $a$ and $b$ are the starting and ending $F$ values of the area over which melt is aggregated and $C_n$ represents the concentration of the quasi-instantaneous melt for $F = n$.

Whole-rock trace element compositions, mineral modes and distribution coefficients after refertilization were recalculated following Appendix B of Hellebrand *et al.* (2002).

Downloaded from http://petrology.oxfordjournals.org/ at Kainan University on March 17, 2015

*Table A1: Source composition and partition coefficients (mineral/melt) used in the model*

| | Ol | Opx | Cpx1 | Cpx2 | Grt | Sp | Source C/C1 |
|---|---|---|---|---|---|---|---|
| SS | 0·57 | 0·21 | | 0·13 | 0·09 | | |
| GM | 0·04 | −0·19 | | 1·05 | 0·11 | | |
| SM | −0·06 | 0·28 | 0·67 | | | 0·11 | |
| Ti | 0·015 | 0·100 | 0·350 | 0·710 | 0·160 | 0·150 | 3·00 |
| Zr | 0·004 | 0·024 | 0·120 | 0·270 | 0·400 | 0·070 | 2·18 |
| La | 0·000007 | 0·0025 | 0·060 | 0·090 | 0·0035 | 0·0006 | 0·91 |
| Ce | 0·00001 | 0·005 | 0·100 | 0·160 | 0·008 | 0·0006 | 1·40 |
| Nd | 0·00007 | 0·010 | 0·200 | 0·360 | 0·050 | 0·0006 | 1·97 |
| Sm | 0·001 | 0·020 | 0·300 | 0·670 | 0·220 | 0·001 | 2·23 |
| Eu | 0·001 | 0·030 | 0·370 | 0·800 | 0·450 | 0·001 | 2·34 |
| Gd | 0·0025 | 0·04 | 0·405 | 0·95 | 1·225 | 0·0015 | 2·39 |
| Dy | 0·004 | 0·050 | 0·440 | 1·100 | 2·000 | 0·002 | 2·44 |
| Er | 0·009 | 0·070 | 0·430 | 1·440 | 3·500 | 0·003 | 2·46 |
| Yb | 0·014 | 0·090 | 0·410 | 1·430 | 5·000 | 0·005 | 2·50 |

Source contents are normalized to C1 chondrite (Anders & Grevesse, 1989). Cpx1, partition coefficients in the spinel field; Cpx2, partition coefficients in the garnet field; SS, source mode; GM, melting mode in the garnet stability field; SM, melting mode in the spinel stability field.

Downloaded from http://petrology.oxfordjournals.org/ at Kainan University on March 17, 2015